

Spin effects and baryon resonance dynamics in ϕ -meson photoproduction at few GeV

A.I. Titov^{ab} and T.-S.H. Lee^c

^a*Advanced Science Research Center,*

Japan Atomic Energy Research Institute, Tokai, Ibaraki, 319-1195, Japan

^b*Bogoliubov Laboratory of Theoretical Physics, JINR, Dubna 141980, Russia*

^c*Physics Division, Argonne National Laboratory, Argonne, Illinois 60439, USA*

Abstract

The diffractive ϕ -meson photoproduction amplitude is dominated by the Pomeron exchange process and contains the terms that govern the spin-spin and spin-orbital interactions. We show that these terms are responsible for the spin-flip transitions at forward photoproduction angles and appear in the angular distributions of $\phi \rightarrow K^+K^-$ -decay in reactions with unpolarized and polarized photon beams. At large momentum transfers, the main contribution to the ϕ -meson photoproduction is found to be due to the excitation of nucleon resonances. Combined analysis of ω and ϕ photoproduction indicates strong OZI-rule violation in ϕNN^* - couplings. We also show that the spin observables are sensitive to the dynamics of ϕ -meson photoproduction at large angles and could help distinguish different theoretical models of nucleon resonances. Predictions for spin effects in ϕ -meson photoproduction are presented for future experimental tests.

PACS numbers: PACS number(s): 13.88.+e, 13.60.Le, 14.20.Gk, 25.20.Lj

I. INTRODUCTION

The photoproduction of light vector meson (ρ, ω, ϕ) is an interesting reaction for many reasons. At high energies ($W \equiv \sqrt{s} \gtrsim 10$ GeV) it brings information on the dynamics of the Pomeron exchange [1, 2, 3, 4, 5, 6, 7, 8]. At low energies ($W \sim 2$ GeV), its observables are sensitive to the resonance channel and can be used to obtain some unique information about the structure of baryon resonances, properties of VNN^* -interactions [9, 10, 11, 12, 13, 14, 15, 16], and possible manifestation of the so-called "missing resonances" [17, 18, 19]. Therefore, the study of vector-meson photoproductions is an important component of the experimental programs at the electron and photon facilities like Thomas Jefferson National Accelerator Facility, the LEPS at SPring-8, ELSA-SAPHIR at Bonn and GRAAL at Grenoble. The ϕ -meson photoproduction at relatively low energies $E_\gamma \simeq 2-3$ GeV plays particularly important role. It is expected that in the diffractive region, the dominant contribution comes from the Pomeron exchange, since trajectories associated with conventional meson exchanges are suppressed by the OZI-rule. The exception is the finite contribution of the pseudoscalar π, η -meson-exchange channel, but its properties are quite well understood [20, 21]. Therefore, the low-energy ϕ -meson photoproduction may be used for studying the presence of additional trajectories. Candidates are trajectories associated with a scalar meson [20, 22] and f'_2 -meson [21] containing a large amount of strangeness, glueball [23] or other exotic channels [24]. But the relative contributions of these additional processes can not be well defined within Regge phenomenology and must be determined from comparisons with experimental data. Spin observables are of crucial importance for such studies. As a matter of fact, the Pomeron exchange amplitude which is inspired by multi-gluon exchange [1] contains specific spin-dependence terms which are negligible in ϕ -meson photoproduction at high energies but become important at a few GeV. These interactions lead to spin-flip processes and give non-trivial behaviour of the spin-density matrix elements even at forward angles. Therefore, the angular distribution of $\phi \rightarrow K^+K^-$ decay can be used as a tool to study the diffractive mechanism, and is complementary to the measurement of unpolarized cross section.

Another subject is related to the strange degrees of freedom in a nucleon. Analysis of magnetic [26, 27] and electroweak [28] moments of baryons show that the ϕ -meson couples more strongly to the nucleon than expected on the basis of the OZI-rule [29]. The presence

of the strange-quark content in the nucleon was indicated by measurements of the π -nucleon term [30], ϕ -meson production in proton annihilation at rest [31, 32, 33] and deep-inelastic electroweak lepton-nucleon scattering (see Ref. [25] for references and a compilation of the data).

The ϕ -meson photoproduction seems to be an effective and promising candidate process for studying the hidden strangeness in a nucleon. The backward-angle photoproduction is dominated by s and u channels of the nucleon and resonant amplitudes and directly related to the strength of ϕNN and ϕNN^* -interactions. The finite - strange content leads to an increase of this strength compared to the expectation based on the standard OZI-rule violation (OZI-rule-evading interaction [22]). This effect must be seen in both unpolarized and spin observables at large momentum transfers.

At forward angles, the nucleon and resonant contributions become negligible for ϕ -meson photoproduction and OZI-rule violation could appear as direct $s\bar{s}$ -knockout [34] from a nucleon. The most promising here is a measurement of spin observables which represent the interference of the weak $s\bar{s}$ -knockout and strong vector-meson dominance photoproduction amplitudes [35, 36, 37]. It is clear that for this purpose the diffractive amplitude must be established unambiguously.

The purpose of this paper is to investigate the problems mentioned above. The main differences with the previous studies of the conventional non-strange amplitude of $\gamma p \rightarrow \phi p$ -reaction [20, 22] are in giving a detailed analysis of the spin properties of the amplitude in diffractive region. We will present a comprehensive analysis of all spin-density matrix elements which are responsible for the angular distributions of K^+K^- in the reaction $\gamma p \rightarrow \phi p$ with unpolarized and polarized photons at a few GeV. For the most important matrix elements we give an estimation in an explicit analytical form, which is useful for the qualitative analysis.

The backward angle photoproduction is described by the nucleon resonance excitations. For the latter, we use an effective Lagrangian approach developed for ω -meson photoproduction [16], where all known nucleon resonances listed in Particle Data Group [38] are included. This resonant model is different from the approach of Ref. [14], which results in giving significantly different predictions of some spin observables.

This paper is organized as follows. In Section II we define the kinematics and observables. Formula for calculation various spin observables are also introduced here. The basic

amplitudes for the conventional processes, such as Pomeron exchange, Reggeon exchanges, and resonance excitations, are given in Section III. In Section IV we discuss results and make predictions for the future experiments. The summary is given in Section V. In Appendix A we discuss an extreme case when the exotic trajectories become dominant in the near-threshold energy region.

II. KINEMATICS AND OBSERVABLES

The scattering amplitude T of the $\gamma p \rightarrow Vp$ reaction (where V can be ϕ or ω) is related to the S -matrix by

$$S_{fi} = \delta_{fi} - i(2\pi)^4 \delta^4(k + p - q - p') T_{fi}, \quad (1)$$

where k , q , p and p' denote the four-momenta of the incoming photon, outgoing vector meson, initial nucleon, and final nucleon, respectively. The standard Mandelstam variables are defined by $t = (p - p')^2 = (q - k)^2$, $s \equiv W^2 = (p + k)^2$, and the vector meson production angle θ by $\cos \theta \equiv \mathbf{k} \cdot \mathbf{q} / |\mathbf{k}| |\mathbf{q}|$. We use convention of Bjorken and Drell to define the γ matrices; the Dirac spinors are normalized as $\bar{u}(p) \gamma_\alpha u(p) = 2p_\alpha$.

The scattering amplitude is written as

$$T_{fi} = \frac{I_{fi}}{(2\pi)^6 \sqrt{2E_\omega(\mathbf{q}) 2|\mathbf{k}| 2E_N(\mathbf{p}) 2E_N(\mathbf{p}')}}, \quad (2)$$

where $E_i(\mathbf{p}) = \sqrt{M_i^2 + \mathbf{p}^2}$ with M_i denoting the mass of the particle i . In the c.m.s. the quantization axis (\mathbf{z}) is chosen along the beam momentum, and the \mathbf{y} -axis is perpendicular to the production plane: $\mathbf{y} = \mathbf{p} \times \mathbf{p}' / |\mathbf{p} \times \mathbf{p}'|$. The differential cross section is related to the invariant amplitude by

$$\frac{d\sigma_{fi}}{dt} = \frac{1}{64\pi(W^2 - M_N^2)^2} \sum_{m_i m_f \lambda_\gamma \lambda_V} |I_{fi}|^2, \quad (3)$$

where m_i, m_f are the proton spin projections in the initial and final state, respectively, and $\lambda_\gamma, \lambda_V$ are the helicities of the incoming photon and outgoing vector meson, respectively. In this paper we will also investigate some of the single and double spin observables [35].

The considered beam asymmetry (Σ_x) for the linearly polarized photons reads

$$\Sigma_x = \frac{d\sigma_{\mathbf{y}} - d\sigma_{\mathbf{x}}}{d\sigma_{\mathbf{y}} + d\sigma_{\mathbf{x}}} = \frac{\text{Tr} \left[I_{fi} \sigma_\gamma^x I_{fi}^\dagger \right]}{\text{Tr} \left[I_{fi} I_{fi}^\dagger \right]}, \quad (4)$$

where the subscript \mathbf{y} (\mathbf{x}) corresponds to a photon linearly polarized along the \mathbf{y} (\mathbf{x}) axis. In the case of a circularly-polarized photon beam, the double beam-target (recoil) asymmetry is very sensitive to the production mechanism [37]. Therefore, in the present work we analyze the beam-target asymmetry

$$C_{zz}^{BT} = \frac{d\sigma(\Rightarrow) - d\sigma(\Leftarrow)}{d\sigma(\Rightarrow) + d\sigma(\Leftarrow)}, \quad (5)$$

where the arrows represent the spin projections of the incoming photon and the target protons: (\Rightarrow) and (\Leftarrow) thus correspond to the initial states with the total spin equal to $\frac{3}{2}$ and $\frac{1}{2}$, respectively.

The double polarization observables related to the beam polarization and polarization of the outgoing vector mesons are described in terms of spin-density matrices ρ_{ij} , which determine the vector-meson decay distributions in its rest frame [39] and are defined by

$$\begin{aligned} \rho_{\lambda\lambda'}^0 &= \frac{1}{N} \sum_{\alpha, \lambda_\gamma} I_{\alpha; \lambda, \lambda_\gamma} I_{\alpha; \lambda', \lambda_\gamma}^\dagger, \\ \rho_{\lambda\lambda'}^1 &= \frac{1}{N} \sum_{\alpha, \lambda_\gamma} I_{\alpha; \lambda, -\lambda_\gamma} I_{\alpha; \lambda', \lambda_\gamma}^\dagger, \\ \rho_{\lambda\lambda'}^2 &= \frac{i}{N} \sum_{\alpha, \lambda_\gamma} \lambda_\gamma I_{\alpha; \lambda, -\lambda_\gamma} I_{\alpha; \lambda', \lambda_\gamma}^\dagger, \\ \rho_{\lambda\lambda'}^3 &= \frac{1}{N} \sum_{\alpha, \lambda_\gamma} \lambda_\gamma I_{\alpha; \lambda, \lambda_\gamma} I_{\alpha; \lambda', \lambda_\gamma}^\dagger, \end{aligned} \quad (6)$$

where the symbol α includes the polarizations of the incoming and the outgoing baryons and the normalization factor reads

$$N = \sum_{\alpha, \lambda, \lambda_\gamma} I_{\alpha; \lambda, \lambda_\gamma} I_{\alpha; \lambda, \lambda_\gamma}^\dagger. \quad (7)$$

The $\phi \rightarrow K^+ K^-$ - decay distribution as a function of the polar (Θ) and azimuthal (Φ) angles is expressed through the spin-density-matrix elements and depends on the beam polarization. The polarization vectors of the linear ($\boldsymbol{\varepsilon}$) and circular ($\boldsymbol{\varepsilon}^\lambda$, $\lambda = \pm 1$) photon polarizations read

$$\begin{aligned} \boldsymbol{\varepsilon} &= (\cos \Psi, \sin \Psi, 0), \\ \boldsymbol{\varepsilon}^\lambda &= -\frac{\lambda}{\sqrt{2}}(1, i\lambda, 0). \end{aligned} \quad (8)$$

For easy reference we list here the explicit form of the decay angular distribution $W(\cos \Theta, \Phi, \Psi)$ for various photon polarizations in the rest frame of the outgoing ϕ -meson. For unpolarized photons it reads

$$W_{\text{unpol.}}(\cos \Theta, \Phi) = W^0(\cos \Theta, \Phi), \quad (9)$$

with

$$W^0(\cos \Theta, \Phi) = \frac{3}{4\pi} \left\{ \frac{1}{2}(1 - \rho_{00}^0) + \frac{1}{2}(3\rho_{00}^0 - 1) \cos^2 \Theta - \sqrt{2} \operatorname{Re} \rho_{10}^0 \sin 2\Theta \cos \Phi - \rho_{1-1}^0 \sin^2 \Theta \cos 2\Phi \right\}. \quad (10)$$

For the circularly-polarized photons of helicity $\lambda_\gamma = \pm 1$ the angular distribution has the following form

$$W^\pm(\cos \Theta, \Phi) = W^0(\cos \Theta, \Phi) \pm \frac{3}{4\pi} P_\gamma \left\{ \sqrt{2} \operatorname{Im} \rho_{10}^3 \sin 2\Theta \sin \Phi + \operatorname{Im} \rho_{1-1}^3 \sin^2 \Theta \sin 2\Phi \right\}, \quad (11)$$

where P_γ is the strength of polarization ($0 \leq P_\gamma \leq 1$).

In the case of the linearly-polarized photons the decay distribution is defined as

$$W^L(\cos \Theta, \Phi, \Psi) = W^0(\cos \Theta, \phi) - P_\gamma (W^1(\cos \Theta, \Phi) \cos 2\Psi + W^2(\cos \Theta, \Phi) \sin 2\Psi), \quad (12)$$

where Ψ denotes the angle between the photon-polarization vector and ϕ -meson production plane (cf. Eq. 8). The partial distributions $W^{1,2}$ read

$$W^1(\cos \Theta, \Phi) = \frac{3}{4\pi} \left\{ \rho_{11}^1 \sin^2 \Theta + \rho_{00}^1 \cos^2 \Theta - \sqrt{2} \operatorname{Re} \rho_{10}^1 \sin 2\Theta \cos \Phi - \rho_{1-1}^1 \sin^2 \Theta \cos 2\Phi \right\}$$

$$W^2(\cos \Theta, \Phi) = \frac{3}{4\pi} \left\{ \sqrt{2} \operatorname{Im} \rho_{10}^2 \sin 2\Theta \sin \Phi + \operatorname{Im} \rho_{1-1}^2 \sin^2 \Theta \sin 2\Phi \right\} \quad (13)$$

Spin-density matrix elements depend on the choice of the quantization axis (\mathbf{z}') which defines the reference frame of the vector meson-decay distribution. There are several choices of the quantization axis \mathbf{z}' in the vector-meson rest frame: the helicity system with \mathbf{z}' opposite to the velocity of the recoiling nucleon, the Gottfried-Jackson system (GJ) with \mathbf{z}' parallel to the momentum of the photon, and the Adair system with \mathbf{z}' parallel to the photon momentum in the c.m.s. Although the general formalism for the analysis of the vector-meson decay does

not depend on the system, all our calculations are done in the GJ system, where some of the amplitudes have a simple helicity-conserving form regardless of the momentum transfers.

Using the two-dimensional decay distribution of Eq. (10), one can get the one-dimensional distributions after integrating over the remaining variables

$$\begin{aligned} W^0(\cos \Theta) &= \frac{3}{2} \left(\frac{1}{2} (1 - \rho_{00}^0) \sin^2 \Theta + \rho_{00}^0 \cos^2 \Theta \right), \\ W^0(\Phi) &= \frac{1}{2\pi} (1 - 2\text{Re}\rho_{1-1}^0 \cos 2\Phi). \end{aligned} \quad (14)$$

In the case of the linearly polarized beam, the distributions depend additionally on the direction of the polarization vector

$$\begin{aligned} W^L(\cos \Theta, \Psi) &= W^0(\cos \Theta) - \frac{3}{2} (\rho_{11}^1 \sin^2 \Theta + \rho_{00}^1 \cos^2 \Theta) P_\gamma \cos(2\Psi), \\ W^L(\Phi, \Psi) &= W^0(\Phi) + \frac{1}{\pi} P_\gamma (\bar{\rho}_{1-1}^1 \cos[2(\Phi - \Psi)] + \Delta_{1-1} \cos[2(\Phi + \Psi)]), \end{aligned} \quad (15)$$

where

$$\bar{\rho}_{1-1}^1 = \frac{1}{2} (\rho_{1-1}^1 - \text{Im}\rho_{1-1}^2), \quad \Delta_{1-1} = \frac{1}{2} (\rho_{1-1}^1 + \text{Im}\rho_{1-1}^2). \quad (16)$$

The averaging over the angle between polarization and production planes, at fixed $\Phi - \Psi$ results in the following one-dimensional distributions

$$\begin{aligned} W^L(\cos \Theta) &= W^0(\cos \Theta), \\ W^L(\Phi - \Psi) &= \frac{1}{2\pi} (1 + 2P_\gamma \bar{\rho}_{1-1}^1 \cos[2(\Phi - \Psi)]). \end{aligned} \quad (17)$$

The integration over Θ and Φ gives dependence of the total decay distribution as a function on Ψ

$$W^L(\Psi) = 1 - P_\gamma (2\rho_{11}^1 + \rho_{00}^1) \cos 2\Psi. \quad (18)$$

For the circularly-polarized beam the distributions read

$$\begin{aligned} W^\pm(\cos \Theta) &= W^0(\cos \Theta), \\ W^\pm(\Phi) &= W^0(\Phi) \pm \frac{1}{\pi} P_\gamma \text{Im}\rho_{1-1}^3 \sin 2\Phi. \end{aligned} \quad (19)$$

We will also discuss the vector-meson decay asymmetry which is related to the matrix elements $\rho_{11}^{0,1}, \rho_{1-1}^{0,1}$

$$\Sigma_V = \frac{\rho_{11}^1 + \rho_{1-1}^1}{\rho_{11}^0 + \rho_{1-1}^0}, \quad (20)$$

and has a meaning of the asymmetry between the two angular distributions when the decay angles are fixed and equal $\Theta = \frac{\pi}{2}$ and $\Phi = \frac{\pi}{2}$, and $\Psi = \frac{\pi}{2}, 0$

$$\Sigma_V = \frac{1}{P_\gamma} \frac{W^L(\cos \Theta, \Phi, \Psi = \frac{\pi}{2}) - W^L(\cos \Theta, \Phi, \Psi = 0)}{W^L(\cos \Theta, \Phi, \Psi = \frac{\pi}{2}) + W^L(\cos \Theta, \Phi, \Psi = 0)}. \quad (21)$$

III. THE AMPLITUDE

A. diffractive photoproduction

The invariant amplitude in the region of small momentum transfers I^{Diff} can be considered in frame of Regge phenomenology as a sum of the Pomeron and other Regge - trajectories. For $E_\gamma \simeq 2 \div 3$ GeV ($s \simeq 5 \div 7$ GeV²) this region is limited by the forward angle photoproduction with $|t| \lesssim 0.5 \div 0.7$ GeV², where $|t|/s \lesssim 0.1 \ll 1$ [40]. As we will see later, the employment of conventional residuals in corresponding amplitudes expressed through the isoscalar nucleon form factors leads to fast decreasing of I^{Diff} , so that it becomes rather small in the region beyond its validity. On the other hand the meson photoproduction at low energy and large momentum transfers with $|t| \sim |t|_{\text{max}}$ ($\theta \sim \pi$) can be described successfully in terms of the nucleon and resonance exchange amplitudes I^{B} . In diffractive region of the ϕ -meson photoproduction I^{B} is suppressed by the OZI-rule and is negligible compared to I^{Diff} . The total amplitude may be written as

$$I_{fi} = I_{fi}^{\text{Diff}} \oplus I_{fi}^{\text{B}} \quad (22)$$

where \oplus means that the above two components are defined and operate in different regions of t and simultaneous account of the Regge-amplitude and the resonant part leads, strictly speaking to double counting [40]. But since in considered case the interference of I^{Diff} and I^{B} at forward and backward angle photoproduction is negligible we can substitute $\otimes \rightarrow +$. This leads to so called "interference model" which was widely used in the resonance region (see for example [42]). But taking into account the problem of double counting at the region of $\theta \sim \frac{\pi}{2}$ when interference of the resonant and Regge-parts may be sizeable, predictions for a such model must be considered as a very qualitative estimations, especially for spin variables.

In the diffractive region of the ϕ -meson photoproduction the two processes are reasonably well established; the Pomeron exchange which is dominant and relatively weak pseudoscalar

π, η -mesons-exchange. For the Pomeron-exchange process, depicted in Fig. 1(a), we use the

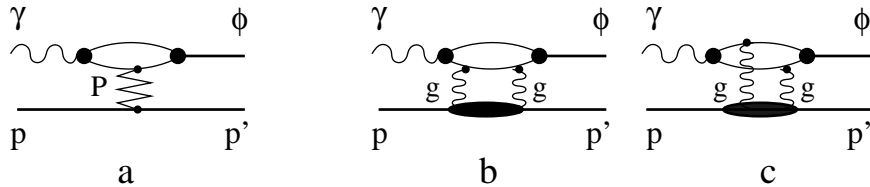


FIG. 1: Diagrammatic representation of (a) Pomeron exchange and (b,c) two gluon-exchange contributions in the $\gamma p \rightarrow \phi p$ reaction.

Donnachie-Landshoff model [1], based on the Pomeron-isoscalar-photon analogy. It gives the amplitude in the following form

$$I_{fi}^P = -M_P(s, t) \Gamma_{fi}^P,$$

$$\Gamma_{fi}^P = \varepsilon_\mu^*(\lambda_V) \bar{u}_f h_P^{\mu\nu} u_i \varepsilon_\nu(\lambda_\gamma), \quad (23)$$

where $\varepsilon_\mu(V)$ and $\varepsilon_\nu(\gamma)$ are the polarization vectors of the vector meson (ω, ϕ) and photon, respectively, and $u_i = u_{m_i}(p)$ ($u_f = u_{m_f}(p')$) is the Dirac spinor of the nucleon with momentum p (p') and spin projection m_i (m_f).

The scalar function $M_P(s, t)$ is described by the following Regge parameterization

$$M_P(s, t) = C_P F_1(t) F_V(t) \frac{1}{s} \left(\frac{s}{s_P} \right)^{\alpha_P(t)} \exp \left[-\frac{i\pi}{2} \alpha_P(t) \right], \quad (24)$$

where $F_1(t)$ is the isoscalar electromagnetic form factor of the nucleon and $F_V(t)$ is the form factor for the vector-meson-photon-Pomeron coupling. We also follow Ref. [1] to write

$$F_1(t) = \frac{4M_N^2 - 2.8t}{(4M_N^2 - t)(1 - t/t_0)^2}, \quad F_V(t) = \frac{2\mu_0^2}{(1 - t/M_V^2)(2\mu_0^2 + M_V^2 - t)}, \quad (25)$$

where $t_0 = 0.7 \text{ GeV}^2$. The Pomeron trajectory is known to be $\alpha_P(t) = 1.08 + 0.25t$. (See also Ref. [7]) The strength factor C_P equal

$$C_P = \frac{6g^2 \sqrt{4\pi\alpha_{\text{em}}}}{\gamma_V}, \quad (26)$$

where γ_V is the vector meson decay constant ($2\gamma_\omega = 17.05$ and $2\gamma_\phi = 13.13$), and $\alpha_{\text{em}} = e^2/4\pi$. The parameter g^2 is the product of two dimensionless coupling constants $g^2 \equiv g_{Pss} \cdot g_{Pqq} = (\sqrt{s_P}\beta_s) \cdot (\sqrt{s_P}\beta_u)$, where g_{Pss} and g_{Pqq} have a meaning of the Pomeron coupling with the strange quarks in a ϕ -meson and the light in a proton, respectively. For the ω -meson photoproduction $g^2 \equiv q_{Pqq}^2$.

The vertex function $h_P^{\mu\nu}$ is defined by a trace calculation of the quark loop in the diagram of Fig. 1(a) with the non-relativistic vector-meson wave function and the vector coupling for the Pomeron-quark-quark vertex ($V_{Pqq} \sim \gamma_\alpha$). The net result reads

$$h_P^{\mu\nu} = \not{k} \left(g^{\mu\nu} - \frac{q^\mu q^\nu}{q^2} \right) - \gamma^\nu \left(k^\mu - \frac{q^\mu k \cdot q}{q^2} \right) - q^\nu \left(\gamma^\mu - \frac{\not{q} q^\mu}{q^2} \right), \quad (27)$$

where we keep the explicit gauge-invariant terms and skip the term proportional to k^ν , which, after being multiplied by the photon polarization vector does not contribute. One can see that the last term violates gauge invariance. That is a serious problem and its solution requires a more detailed description of the gluon-exchange mechanism and vertex functions [5, 6, 47], which is beyond the scope of this work. Here, we perform gauge-invariance restoration by gauge transformation, since the above described simple model has been so successful in description of many processes. The easiest way is transformation of q^ν in the last term of Eq. (27)

$$q^\nu \rightarrow \bar{q}^\nu = q^\nu - \bar{p}^\nu \frac{k \cdot q}{\bar{p} \cdot k}. \quad (28)$$

where the vector \bar{p} must be fixed via an additional assumption. Using this transformation the vertex function Γ_{fi}^P has the following form

$$\Gamma_{fi}^P = \bar{u}_f \not{k} u_i (\varepsilon_{\lambda_V}^* \cdot \varepsilon_{\lambda_\gamma}) - \bar{u}_f \not{\varepsilon}_{\lambda_\gamma} u_i (\varepsilon_{\lambda_V}^* \cdot k) - \bar{u}_f \not{\varepsilon}_{\lambda_V}^* u_i \left(\varepsilon_{\lambda_\gamma} \cdot q - \frac{(\varepsilon_{\lambda_\gamma} \cdot \bar{p})(k \cdot q)}{\bar{p} \cdot k} \right). \quad (29)$$

To find the vector \bar{p} we take into account that it must lie in the production plane and be constructed from the three linear independent vectors p, p' and q , be different from q and, it must has a proper "high energy limit". This limit may be find using the using the Pomeron - two-gluon-exchange analogy [43], since it is now generally believed that the Pomeron exchange is generated by the gluon exchange [44, 45] and the non-perturbative two-gluon-exchange process [2] justifies the vector type of coupling in Pqq -vertex.

The two-gluon exchange amplitude for the vector meson photoproduction is depicted in Fig. 1(b, c). The amplitude, where the two gluons interact with the same quark (Fig. 1(b)) generates the vertex $h_{2g}^{\mu\nu}$ with the same structure as the Pomeron-exchange mechanism. The amplitude where the two gluons interact with different quarks (Fig.1(c)) contains an additional term proportional to $\bar{u}(p') \not{\varepsilon}_{\lambda_\gamma} u(p_1) \cdot \bar{u}(p_1) \not{\varepsilon}_{\lambda_V}^* u(p)$, where p_1 is the momentum of the quark in the intermediate state. This term restores the gauge invariance. At high

energies and small momentum transfers where $p' \simeq p_1 \simeq p$ and $\bar{u}(p')\gamma_\alpha u(p) \simeq 2p_\alpha$, the two-gluon-exchange model results [46, 47]

$$\Gamma_{fi}^{2g} \sim (k \cdot p)(\varepsilon_{\lambda_V}^* \cdot \varepsilon_{\lambda_\gamma}) - (\varepsilon_{\lambda_\gamma} \cdot p)(\varepsilon_{\lambda_V}^* \cdot k) - (\varepsilon_{\lambda_V}^* \cdot p) \left(\varepsilon_{\lambda_\gamma} \cdot q - \frac{(\varepsilon_{\lambda_\gamma} \cdot p)(k \cdot q)}{p \cdot k} \right). \quad (30)$$

One can see the identity of Eqs. (29) and(30) and if $\bar{p} = p$ (cf. Ref. [21]). But at relatively low energies where $p' \neq p$, a more reasonable choice is $\bar{p} = \frac{1}{2}(p + p')$, symmetrical with respect of p and p' , because of an approximate estimates $\bar{u}(p')\gamma_\alpha u(p) \simeq (p + p')_\alpha$. This value of \bar{p} , together with Eq. (29) will be used in our calculations. Note, that at large photon energies, the last two terms in (29) is negligible, but at a few GeV and finite $|t|$ they generate spin-flip transitions and become important.

By fitting all available total cross section data for ω , ρ , and ϕ photoproduction at high energies, the remaining parameters of the model are determined: $\mu_0^2 = 1.1 \text{ GeV}^2$, $s_P = 4 \text{ GeV}^2$, and $\beta_s = 1.61$ and $\beta_u = 2.05 \text{ GeV}^{-1}$, which give $g_{Pqq} = 4.1$ and $g_{Pss} = 3.22$.

The pseudoscalar-meson-exchange amplitude may be expressed either in terms of the one-boson-exchange model [10, 20, 22, 37] or using the Regge model [21, 24]. The pseudoscalar-meson exchange amplitude in the one-boson-exchange (OBE) approximation is evaluated from the following effective Lagrangians

$$\begin{aligned} \mathcal{L}_{V\gamma\varphi} &= \frac{eg_{V\gamma\varphi}}{M_V} \epsilon^{\mu\nu\alpha\beta} \partial_\mu V_\nu \partial_\alpha A_\beta \varphi, \\ \mathcal{L}_{\varphi NN} &= -ig_{\pi NN} \bar{N} \gamma_5 \tau_3 N \pi^0 - ig_{\eta NN} \bar{N} \gamma_5 N \eta, \end{aligned} \quad (31)$$

where $\varphi = (\pi^0, \eta)$ and A_β is the photon field. The resulting invariant amplitude is

$$I_{fi}^{ps} = - \sum_{\varphi=\pi,\eta} \frac{iF_{\varphi NN}(t)F_{V\gamma\varphi}(t)}{t - M_\varphi^2} \frac{eg_{V\gamma\varphi}g_{\varphi NN}}{M_V} \bar{u}_{m_f}(p')\gamma_5 u_{m_i}(p) \epsilon^{\mu\nu\alpha\beta} q_\mu k_\alpha \varepsilon_\nu^*(V) \varepsilon_\beta(\gamma). \quad (32)$$

In the above, we have followed Ref. [48] to include the following form factors to dress the φNN and $V\gamma\varphi$ vertices,

$$F_{\varphi NN}(t) = \frac{\Lambda_\varphi^2 - M_\varphi^2}{\Lambda_\varphi^2 - t}, \quad F_{V\gamma\varphi}(t) = \frac{\Lambda_{V\gamma\varphi}^2 - M_\varphi^2}{\Lambda_{V\gamma\varphi}^2 - t}. \quad (33)$$

We use $g_{\pi NN} = 13.26$ and $g_{\eta NN} = 3.527$ for the πNN and ηNN coupling constants, respectively (cf. Ref. [20] for discussion and references). The coupling constants $g_{V\gamma\varphi}$ can be estimated through the decay widths of $V \rightarrow \gamma\pi$ and $V \rightarrow \gamma\eta$ [38] which lead to $g_{\omega\gamma\pi} = 1.823$, $g_{\phi\gamma\pi} = -0.141$, $g_{\omega\gamma\eta} = 0.416$ and $g_{\phi\gamma\eta} = -0.707$. The cutoff parameters Λ_φ and $\Lambda_{\omega\gamma\varphi}$ in

Eq. (33) are chosen to reproduce the ω -meson photoproduction at low energies [16]: $\Lambda_\pi = 0.6$ GeV², $\Lambda_\eta = 0.9$ GeV², $\Lambda_{V\gamma\pi} = 0.6$ GeV² and $\Lambda_{V\gamma\eta} = 1.0$ GeV².

In Refs. [21, 24, 49] it is suggested to describe pseudoscalar-meson (PS) exchange with a π -meson-exchange trajectory by making use of Reggeization of the Feynman propagator in the following way

$$\frac{1}{t - m_\pi^2} \implies \left(\frac{s}{s_1}\right)^{\alpha_\pi(t)} \frac{(1 + e^{-i\pi\alpha_\pi(t)})\pi\alpha'_\pi}{2 \sin(\pi\alpha_\pi) \Gamma(\alpha_\pi(t) + 1)}, \quad (34)$$

where the trajectory is given by

$$\alpha_\pi(t) = \alpha'_\pi(t - m_\pi^2), \quad (35)$$

with $\alpha'_\pi = 0.7$ GeV⁻². Using properties of the Γ -function: $\Gamma(1+z) = z\Gamma(z)$ and $\Gamma(z)\Gamma(1-z)\sin\pi z = \pi$, and assuming that $|\alpha_\pi(t_{\max})| \ll 1$ one can see that the Reggeization of Eq. (34) does not modify the pole t -dependence of the OBE amplitude at forward-angle photoproduction. The Regge phenomenology does not define t -dependence and phases of residuals. In practice, they are determined by comparison of the Regge and OBE-amplitudes at low energies where the lowest t -channel resonances are expected to be dominant [41, 49]. In the present paper we analyze photoproduction in narrow energy region for $W = 2 \sim 3$ GeV and in order to avoid consideration of additional parameters we will use directly the OBE model for the pseudoscalar-meson-exchange processes, with the parameters taken from independent studies. In this case our result coincides with the Regge model at small $|t|$ and slightly overestimates it at backward-angle photoproduction where the contribution of pseudoscalar-meson-exchange becomes negligible relative to the other channels.

Together with these conventional processes, several other diffractive channels are discussed in literature. One of them is OZI-rule allowed f'_2 meson exchange or contribution of the f'_2 -meson Regge trajectory [21]. Significant strangeness content of $f'_2(1525)$ supports existence of this channel. But, on the other hand, the absence of a finite $f'_2 \rightarrow \gamma\phi$ decay width [38] is a real problem for applying of a f'_2 -trajectory in ϕ -meson photoproduction and the only argument for its use is to obtain agreement with the low-energy data.

Another possible low-energy channel is related to the pure gluon dynamics like a glueball exchange or the contribution of a glueball ($J^\pi = 0^+$, $M_{\text{gl}}^2 \simeq 3$ GeV²) inspired trajectory [23]. The idea is based on assumption that the Pomeron trajectory is also inspired by the glueball exchange, being the leading glueball Regge trajectory. Other trajectories may appear as its

daughter trajectories. This picture has been justified recently by calculations within the string model [8, 50]. The slope of the glueball trajectory is found to be much smaller than slope of conventional mesonic trajectories and close to the Pomeron trajectory.

Since both f'_2 and glueball trajectories are not forbidden, we also include them into the total amplitude. To fix the vertex ($h^{\mu\nu}$) we use the simplest covariant and gauge invariant effective Lagrangians for $VV\xi$ interacting where V and ξ are the vector and boson (0^+ , 2^+) fields, respectively:

$$\mathcal{L}_{0^+} = \frac{1}{4} g_{\alpha\beta} (\Lambda^{\alpha\beta} + \Lambda^{\beta\alpha}) \xi \quad (36a)$$

$$\mathcal{L}_{2^+} = \frac{1}{4} (\Lambda^{\alpha\beta} + \Lambda^{\beta\alpha}) \xi_{\alpha\beta} + (\Lambda^{\alpha\beta} - \Lambda^{\beta\alpha}) \xi_{\alpha\beta}, \quad (36b)$$

with

$$\Lambda^{\alpha\beta} = \partial_\mu V_1^\alpha \partial^\mu V_2^\beta + \partial^\alpha V_1^\mu \partial^\beta V_{2\mu} - \partial^\alpha V_1^\mu \partial_\mu V_2^\beta - \partial_\mu V_1^\alpha \partial^\beta V_2^\mu. \quad (37)$$

Taking the corresponding fermion-boson interactions as $\bar{\psi}\psi\xi$ and $\bar{\psi}\gamma^\alpha\gamma^\beta\psi\xi_{\alpha\beta}$, we get the vertices ($h^{\mu\nu}$) as following

$$h_{0^+}^{\mu\nu} = g^{\mu\nu} k \cdot q - k^\mu q^\nu, \quad (38a)$$

$$h_{2^+}^{\mu\nu} = h_{0^+}^{\mu\nu} - 2i\sigma_{\alpha\beta} [g^{\alpha\mu} g^{\beta\nu} k \cdot q + q^\alpha k^\beta g^{\mu\nu} + g^{\alpha\nu} q^\beta k^\mu + g^{\beta\mu} k^\alpha q^\nu] \quad (38b)$$

Note, that the similar expressions can be also found using the loop integration within the same prescription as for the Pomeron exchange in the Donnachie-Landshoff model with the Reggeon-quark-quark vertices taken as 1 and $\gamma_\alpha\gamma_\beta$ for 0^+ and 2^+ -exchanges, respectively. The difference is in additional gauge breaking term which appears in (38b): $g^{\alpha\mu} q^\beta q^\nu$. It brings some ambiguity for this method, but for us it is important that the structure of all other terms, including their mutual signs is identical to (38b).

The scalar ($M(s, t)$)- functions read

$$M_R(s, t) = C_R F_1(t) F_V(t) \frac{1}{N_R} \left(\frac{s}{s_R} \right)^{\alpha_R(t)} \frac{\eta_R (1 + e^{-i\pi\alpha_R(t)}) \pi \alpha'_R}{2 \sin(\pi\alpha_R) \Gamma(\alpha_R(t))}, \quad (39)$$

where $R = f'_2, gl$ and C_R differ from C_P in (24) by substitution $g_P^2 \rightarrow g_R^2$. The normalization factors N_R in (23) are defined by h_R : $N_{2^+} \simeq 2sM_V$, $N_{0^+} \simeq M_N M_V^2$. Following Ref.[21] we choose f'_2 trajectory as $\alpha_{f'_2} = 0.55 + \alpha'_{f'_2} t$, with $\alpha_{f'_2} = 0.7 \text{ GeV}^{-2}$ and the mass scale $s_{f'_2} = 1 \text{ GeV}^2$. For the glueball trajectory we will use parameters of Ref [23] with $\alpha_{gl}(0) = -0.75$

and $\alpha'_{gl} = 0.25 \text{ GeV}^{-2}$ and $s_{gl} = \alpha'_{gl}^{-1}$. Phase $\eta_R = \pm 1$ and strength g_R are not defined in the Regge model and have to be found to bring the model calculation close to the data for unpolarized total cross section.

Finally, we note that sometimes in literature the Regge amplitude at low energy is chosen with an additional threshold factor to get a better shape of the energy dependence in the near-threshold region, which modifies the standard parameterization as follows

$$\left(\frac{s}{s_R}\right)^{\alpha(t)} \rightarrow \left(\frac{s - a_R}{s_R}\right)^{\alpha(t)}. \quad (40)$$

It is obvious, that relative contribution of each trajectory in the threshold region strongly depends on the threshold parameter a_R , which is not defined by the Regge model. Thus, the finite value of a_P in Pomeron exchange leads to a decrease of the contribution of the Pomeron exchange-amplitude, which must be compensated by the increase of strength in additional trajectories [20, 22, 23]. The shape of the energy dependence of the total cross section is sensitive to the choice of a_P , a_R at energies close to the threshold. In the present paper we choose the value $a_R = 0$ for all trajectories. This choice corresponds to the upper limit for contribution of Pomeron exchange and the lower limit for the additional Regge trajectories in near-threshold region. Its validity must be checked in study of the polarization observables in diffractive region, because the vertex functions for the Pomeron and other trajectories in Eqs. (29), (38a) and (38b) lead to quite different predictions. In Appendix A we illustrate this point for two other extreme cases when the diffractive amplitude is dominated by the f'_2 and 0^+ (glueball)-trajectories, respectively. They can be realized at large a_P : $a_P \sim s_P$.

B. baryon and baryon resonances exchange

The amplitude I^B in Eq. (22) consist of baryon I^N and baryon-resonance-exchange I^{N^*} terms

$$I^B = I^N + I^{N^*}. \quad (41)$$

To evaluate these channels we use the effective Lagrangian approach, developed for ω -meson photoproduction and discussed in our recent paper [16]. Here, we restrict the consideration to a brief description, given below. We consider all isospin $I = 1/2$ nucleon resonances listed by PDG [38] with empirically known helicity amplitudes of $\gamma N \rightarrow N^*$ transitions. We thus have

contributions from 12 resonances: $P_{11}(1440)$, $D_{13}(1520)$, $S_{11}(1535)$, $S_{11}(1650)$, $D_{15}(1675)$, $F_{15}(1680)$, $D_{13}(1700)$, $P_{11}(1710)$, $P_{13}(1720)$, $F_{17}(1990)$, $D_{13}(2080)$, and $G_{17}(2190)$.

In Ref. [16] we found that the contribution of the nucleon term is much smaller than a resonant part. Therefore, in present paper we only consider the resonance-exchange contribution.

For the N^* with spin (J) and parity (P) $J^P = \frac{1}{2}^\pm, \frac{3}{2}^\pm, \frac{5}{2}^\pm, \frac{7}{2}^\pm$, we use the following effective Lagrangians:

$$\mathcal{L}_{\gamma NN^*}^{\frac{1}{2}^\pm} = \frac{eg_{\gamma NN^*}}{2M_{N^*}} \bar{\psi}_{N^*} \Gamma^{(\pm)} \sigma_{\mu\nu} F^{\mu\nu} \psi_N + \text{h.c.}, \quad (42)$$

$$\mathcal{L}_{\gamma NN^*}^{\frac{3}{2}^\pm} = i \frac{eg_{\gamma NN^*}}{M_{N^*}} \bar{\psi}_{N^*}^\mu \gamma_\lambda \Gamma^{(\mp)} F^{\lambda\mu} \psi_N + \text{h.c.}, \quad (43)$$

$$\mathcal{L}_{\gamma NN^*}^{\frac{5}{2}^\pm} = \frac{eg_{\gamma NN^*}}{M_{N^*}^2} \bar{\psi}_{N^*}^{\mu\alpha} \gamma_\lambda \Gamma^{(\pm)} (\partial_\alpha F^{\lambda\mu}) \psi_N + \text{h.c.}, \quad (44)$$

$$\mathcal{L}_{\gamma NN^*}^{\frac{7}{2}^\pm} = -i \frac{eg_{\gamma NN^*}}{M_{N^*}^3} \bar{\psi}_{N^*}^{\mu\alpha\beta} \gamma_\lambda \Gamma^{(\mp)} (\partial_\beta \partial_\alpha F^{\lambda\mu}) \psi_N + \text{h.c.}, \quad (45)$$

where ψ_N is the nucleon fields, ψ_{N^*} , ψ_α , $\psi_{\alpha\beta}$, and $\psi_{\alpha\beta\gamma}$ are the Rarita-Schwinger spin $\frac{1}{2}$, $\frac{3}{2}$, $\frac{5}{2}$ and $\frac{7}{2}$ field, respectively, M_{N^*} is the resonance mass; A_μ is the photon field, and $F^{\mu\nu} = \partial^\nu A^\mu - \partial^\mu A^\nu$. The coupling $\Gamma^+ = 1(\Gamma^- = \gamma_5)$ defines the N^* excitations with different parity.

We define the ωNN^* interactions by using the vector-dominance model. This assumes that the effective $\mathcal{L}_{\omega NN^*}$ Lagrangian has the same form as the corresponding $\mathcal{L}_{\gamma NN^*}$ with substitutions $A_\mu \rightarrow \omega_\mu$ and $eg_{s\gamma NN^*} \rightarrow f_\omega$, where $f_\omega = 2g_s\gamma_\omega$. The isoscalar-coupling constant g_s is related to the strengths of the N^* excitations on the proton ($g_p = g_{\gamma p N^*}$) and on the neutron ($g_n = g_{\gamma n N^*}$) and equals $g_s = (g_p + g_n)/2$.

The γNN^* and ωNN^* vertices are regularized by the form factor $F_{N^*}(r^2) = \Lambda^4/(\Lambda^4 + (r^2 - M_{N^*}^2)^2)$, where r is the four-momentum of the intermediate baryon state, the cut-off parameter $\Lambda = 0.85$ GeV is chosen to be the same for all resonances. More detailed discussion of the effective Lagrangians, propagators, fixing the γNN^* couplings and comparison with other approaches is given in Ref. [16]. Validity of the model is illustrated by Fig. 2, where we show result of our calculation for the differential cross section of $\gamma p \rightarrow \omega p$ reaction together with experimental data at $E_\gamma = 1.23, 1.68$ GeV [53] and 3.65 GeV [54]. In Fig. 2(a) we show the differential cross section as a function of t at $E_\gamma = 1.68$ GeV (solid curve) together with the partial contribution of each of the main channels: pseudoscalar-meson exchange, Pomeron exchange, and resonance excitation, depicted by long-dashed, dot-dashed, and

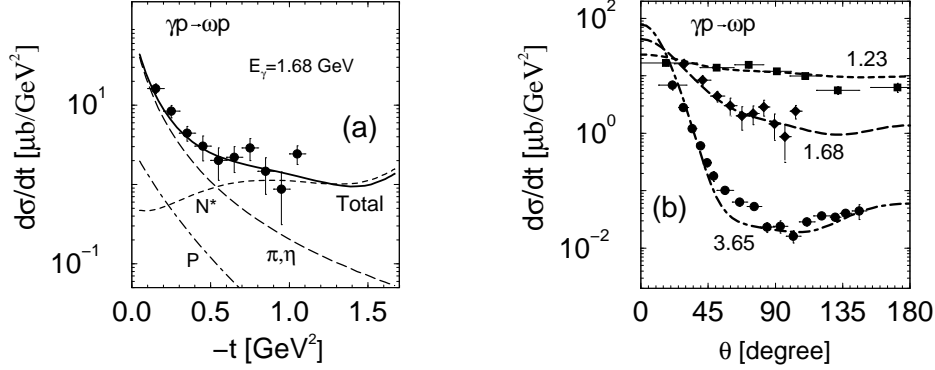


FIG. 2: (a): The differential cross section of $\gamma p \rightarrow \omega p$ reaction as a function of $-t$ at $E_\gamma = 1.68$ GeV. The lines denote the pseudoscalar-meson exchange (long dashed), Pomeron exchange (dot-dashed), resonant channel (dashed), and the full amplitude (solid), respectively. (b): The differential cross sections a function of the ω -meson production angle at $E_\gamma = 1.23, 1.68$ GeV and 3.65 GeV. Data are taken from Refs. [53, 54].

dashed curves, respectively. In Fig. 2(b) we show the differential cross section as a function of the ω production angle in c.m.s. at $E_\gamma = 1.23, 1.68$ and 3.65 GeV by the dashed, dot-dashed and solid lines, respectively. The contribution of the resonance excitations is important at backward angles and it results in the agreement of data with our calculation at large momentum transfers. We also found that at $E_\gamma=3.65$ GeV the Pomeron-exchange contribution only is not sufficient to get agreement at forward angle photoproduction with $|t| < 1$ GeV². Therefore, following Ref. [21], we include also a f_2 -meson trajectory. It is calculated similarly to the f'_2 -meson trajectory (Eqs.(39)) with $g_{f_2}^2 \simeq 3g_P^2$ and $\eta_{f_2} = +1$. One can see, that the model satisfactory reproduces both the energy and the angular distribution of the ω photoproduction in the considered energy region. However, it leaves some windows for additional processes, like two-step photoproduction mechanisms [55] and direct-quark exchange, which is expected to be important at large energy and $\theta \sim \pi/2$ [54] and must be subject for special detailed analysis. There, it is most important that the model reproduces the cross section at backward angle photoproduction, which allows us to fix the resonant part of the ϕ -meson photoproduction.

For the ϕ -meson photoproduction we assume the same N^* -excitation mechanism with the substitution $f_{\omega NN^*} \rightarrow f_{\phi NN^*}$. The key problem is how to fix these coupling constants.

For this aim we use the "minimal" parameterizations of the ϕNN^* coupling constants

$$f_{\phi NN^*} = -\tan \Delta\theta_V x_{\text{OZI}} f_{\omega NN^*}, \quad (46)$$

where $\Delta\theta_V$ is the deviation of the $\phi-\omega$ mixing angle from the ideal mixing ($\Delta\theta_V \simeq 3.7^\circ$ [38]) and x_{OZI} is the OZI-rule evading parameter [22], which will be found from comparison of calculation and data at large momentum transfers. Enhancement of x_{OZI} from 1 determines the scale of the OZI-rule violation in interaction of the ϕ -meson with baryons.

IV. RESULTS AND DISCUSSIONS

A. unpolarized cross sections

We first consider the total cross section. Its dominant contribution comes from the diffractive channels at $|t| < 1 \text{ GeV}^2$. The resonance excitations which are important at large $|t|$ do not affect the total cross section. The total cross section data allow a wide range of OZI-rule evading parameter of the ϕNN^* couplings defined in Eq.(44). Therefore, for definiteness sake, we take $x_{\text{OZI}} = 4$, which is close to its low bound reported in [31, 32, 33] and as we will see later, this value is in agreement with the available data on ϕ -meson photoproduction at large momentum transfers.

For the analysis of the diffractive mechanism we have to keep in mind that the Pomeron (P) and pseudoscalar (PS) meson-exchange are well established. Therefore, any "exotic" process is included as a supplementary channel. We will analysis three possibility: the model I includes the Pomeron (P) and pseudoscalar meson exchange (PS) (i.e. without exotic channel); model II includes P and PS-meson exchange and f'_2 Regge trajectory; model III includes P+PS-meson exchange and the glueball inspired trajectory.

All formula for the models I-III have been described above. The strength parameter g_R and phase factor η_R of f'_2 -meson and glueball trajectories are fixed by fitting the available data: $g_{f'_2} = 1.87, \eta_{f'_2} = +1; g_{gl} = 7.66, \eta_{gl} = -1$.

In Fig. 3(a) we show the total cross section of $\gamma p \rightarrow \phi p$ reaction as a function of the photon energy for three models together with the available experimental data [57, 58]. Comparison with the data slightly favors for the models II and III, but unfortunately, the accuracy of the data is not sufficient to make a definite conclusion about the preference for one of the models. The difference between the models disappears at high energy with $W \gtrsim 10 \text{ GeV}$ ($E_\gamma \gtrsim 50$

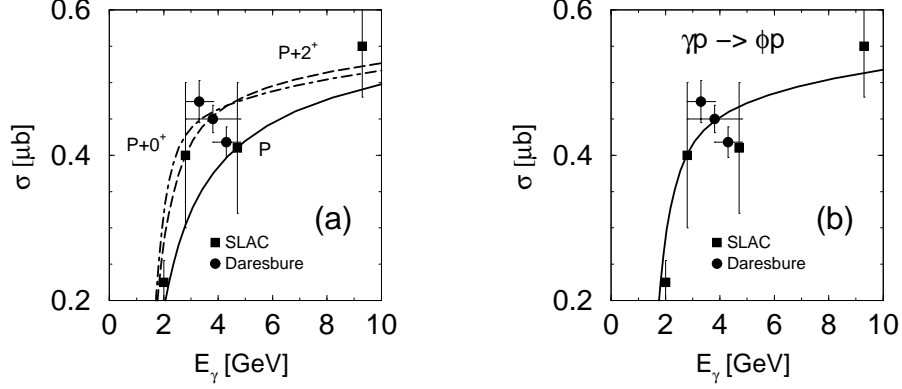


FIG. 3: (a): The total cross section of $\gamma p \rightarrow \phi p$ reaction as a function of the photon energy E_γ for the models I, II and III indicated by dashed, long-dashed and dot-dashed curves, respectively. Data are taken from Ref. [57, 58]. (b): The total cross section for the hybrid model.

GeV), were only the Pomeron trajectory is important. At low energy, high precision data are required to select the favored diffractive mechanism. Taking into account some ambiguity for the reaction mechanism, all our calculations will be done using the "hybrid" model, where the amplitude is taken as a sum of the Pomeron and PS-meson-exchange amplitudes and small contribution of the f'_2 and glueball trajectories taken with the equal weights with: ($g_{f'_2} = 1.32$ and $g_{gl} = 5.42$). The total cross sections calculated from this hybrid model is shown in Fig. 3(b). In the further discussions, for simplicity, we will denote the sum of Pomeron-, f'_2 - and glueball-exchange amplitudes as the "diffractive" amplitude. The opposite case when the f'_2 or 0^+ -exchange trajectories are dominant is discussed in Appendix A.

In $\gamma p \rightarrow \omega p$ reaction at low energies the backward-angle photoproduction is dominated by the resonant channel (cf. Fig. 2) and we expect a similar picture for $\gamma p \rightarrow \phi p$ reaction. The global structure of N^* -exchange amplitude is fixed by the ω -meson photoproduction and the remaining parameter for the ϕ -meson photoproduction is the OZI-rule evading parameter x_{OZI} in Eq. (46). Fig. 4 shows the differential cross section at $E_\gamma = 3.6$ GeV as a function of t for different values of x_{OZI} , together with experimental data [60]. The calculation brings agreement with data at $x_{OZI} \simeq 4$. This value is consistent with results reported in Refs. [31, 32, 33] and the estimation of Refs. [27, 28]. It would be interesting to check this prediction at lower energies, where the relative contribution of the resonant

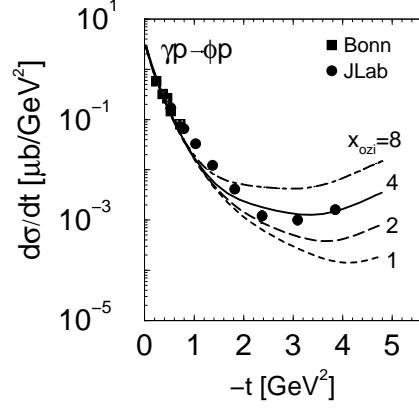


FIG. 4: The differential cross section of $\gamma p \rightarrow \phi p$ reaction as a function of t at $E_\gamma = 3.6$ GeV for different values of the OZI-rule evading parameter x_{OZI} . Data are taken from Refs. [60].

channels is expected to be stronger.

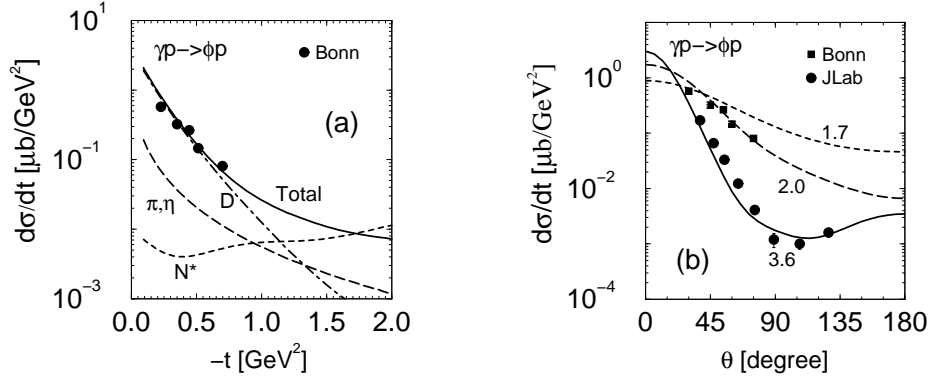


FIG. 5: (a): The differential cross section of $\gamma p \rightarrow \phi p$ reaction as a function of $-t$ at $E_\gamma = 2.2$ GeV. The results are the pseudoscalar-meson exchange (long dashed), diffractive channels (dot-dashed), and resonance excitation (dashed), and the full amplitude (solid). (b): The differential cross section a function of the ϕ -meson production angle at $E_\gamma = 1.7, 2.0$ and 3.6 GeV. Data are taken from Ref. [59, 60].

In Fig. 5(a) we show the differential cross section as function of t at $E_\gamma = 2.0$ GeV together with the partial contribution of main channels with $x_{OZI} = 4$. The diffractive part is described by the hybrid model. One can see that the forward-angle photoproduction is completely defined by the diffractive amplitude; the contribution from the diffractive channels exceeds the pseudoscalar meson exchange by an order of magnitude. Backward-

angle photoproduction is dominated by the N^* -exchange channel, while in the central region ($0.7 \lesssim |t| \lesssim 1.4 \text{ GeV}^2$), the coherent interference of all processes becomes important. Unfortunately, our model is not very well defined in this region. Fig. 5(b) shows the differential cross section as a function of the ϕ -meson production angle in the c.m.s. at $E_\gamma = 1.7, 2.0$ and 3.6 GeV (dashed, long dashed and dot-dashed lines, respectively). The calculations are in agreement with available data. Since the data at $E_\gamma = 3.6 \text{ GeV}$ are used to fix x_{OZI} , the other curves represent our prediction which would be interesting to check.

B. spin observables

Spin observables can be used as a powerful tool to test the photoproduction mechanisms in detail. We first consider the spin-density matrix elements $\rho_{\lambda\lambda'}^{0-3}$, which are planned to be measured in near future at JLab [61] and at LEPS/SPring-8 [62]. All our calculation has been done in the Gottfried-Jackson system. For simplicity, we show our prediction at all momentum transfers, however the applicability of the model at $E_\gamma \sim 2 - 3 \text{ GeV}$ is limited by the forward and backward photoproduction with $|t_{\min}| \leq |t| \leq |t_l|$ and $|t_l| \leq |t| \leq |t|_{\max}$, respectively, where $|t_l| \simeq 0.5 - 0.7 \text{ GeV}^2$, depending on the energy.

First of all, we remind that the non-zero spin-density matrix elements for the pure helicity conserving amplitude:

$$I_{fi} \sim \delta_{\lambda_i \lambda_f} \delta_{m_i m_f} \quad (47)$$

have the following values

$$\begin{aligned} \rho_{11}^0 &= \rho_{-1-1}^0 = \frac{1}{2}, & \rho_{1-1}^1 &= \rho_{-11}^1 = \pm \frac{1}{2}, \\ \text{Im}\rho_{-11}^2 &= -\text{Im}\rho_{1-1}^2 = \pm \frac{1}{2}, & \rho_{11}^3 &= -\rho_{-1-1}^3 = \pm \frac{1}{2}, \end{aligned} \quad (48)$$

where the upper and lower signs in $\rho^{1,2,3}$ correspond to the amplitudes with natural (I^N) and unnatural (I^U) parity exchange, respectively. The typical example of the natural and unnatural parity exchange amplitude in our case are the scalar and the pseudoscalar-meson exchange amplitudes, respectively. For the forward-angle photoproduction they can be expressed as

$$I_{m_f m_i; \lambda_\phi \lambda_\gamma}^N(t) = \begin{pmatrix} 1 \\ 2m_i \lambda_\gamma \end{pmatrix} \delta_{m_i m_f} \delta_{\lambda_\gamma \lambda_\phi} I_0^N(t),$$

where $I_0^{\text{U}}(t)$ is the spin-independent part of the corresponding amplitudes.

The Pomeron-exchange amplitude in GJ-system has the following structure

$$I_{fi}^P \sim -\delta_{\lambda_\phi \lambda_\gamma} \bar{u}_f \not{k} u_i + \delta_{\lambda_\phi 0} k_\gamma \bar{u}_f \not{\epsilon}_{\lambda_\gamma} u_i + \sqrt{2} \lambda_\gamma p_x \frac{k \cdot q}{2p \cdot k - k \cdot q} \bar{u}_f \not{\epsilon}_{\lambda_\phi}^* u_i, \quad (49)$$

where k_γ and p_x are the photon momentum and the x -component of the proton ($p_x = p'_x$ in GJ-system) momentum, respectively. One can see, that only the first term satisfies (47). The second term describes the interaction of the photon and nucleon spins and the interaction of the ϕ -meson spin and the orbital momentum in the initial state. The third term is responsible for the interaction of the ϕ -meson and nucleon spins and for the interaction of the photon spin with the orbital momentum in the final state. At $E_\gamma = 2 - 3$ GeV, contribution of these two terms is finite and must be taken into account. Thus, the second and third terms in Eq. (49) are responsible for the spin-flip transitions $\lambda_\gamma \rightarrow \lambda_\phi = 0$ and generate finite value of ρ_{00}^0 . The contribution of the second term is dominant and it can be estimated as

$$\rho_{00}^0 \simeq \frac{k_\gamma^2 (|t| + 2p_x^2)}{\bar{s}^2},$$

$$\bar{s}^2 = (s - M_N^2)^2 \left(1 - \frac{M_\phi^2 + |t|}{s - M_N^2} \right). \quad (50)$$

This equation shows that ρ_{00}^0 increases monotonically with $|t|$ and at $E_\gamma = 2.2$ GeV and at $\theta = \pi$ reaches large value of $\rho_{00}^0 \simeq 0.6$.

The interaction of the photon spin with the orbital momentum is responsible for so-called double spin-flip transition $\lambda_\gamma \rightarrow \lambda_\phi = -\lambda_\gamma$ and generates ρ_{1-1}^0 , which is defined by the interference of the first and third terms in Eq. (49)

$$\rho_{1-1}^0 \simeq \frac{p_x^2 (M_\phi^2 + |t|)}{\bar{s}^2}. \quad (51)$$

This matrix element reaches its maximum value $\rho_{1-1}^0 \simeq 0.2$ at $|t| \simeq 1$ GeV² and $E_\gamma = 2.2$ GeV. Note, that this matrix element depends on the choice of the gauge parameter $\bar{p} = ap + bp'$ in Eq. (28) with constrains $a, b > 0$ and $a + b = 1$, which provide the proper high energy limit. Our choice is $a = b = \frac{1}{2}$. ρ_{1-1}^0 is proportional to $\varepsilon_\lambda(\gamma) \cdot \bar{p} / (s - M_N^2 - b(M_\phi^2 + |t|))$. Since in GJ-system $p_x = p'_x$, then the product $\varepsilon_\lambda(\gamma) \cdot \bar{p} = \sqrt{2} \lambda p_x$ does not depend on this choice. The rest dependence on choice of \bar{p} is rather weak. Thus, at $E_\gamma = 2.2$ GeV the choice of $a = 1, b = 0$ ($a = 0, b = 1$) results in decrease (increase) of ρ_{1-1}^0 by a factor of 20%.

The resonant channel and f'_2 -trajectory (first and third terms in the brackets in(38b)) also generate the finite spin-flip matrix elements, but in the region with $|t| < 1 \text{ GeV}^2$ their contribution to ρ_{00}^0 , ρ_{1-1}^0 is about of an order of magnitude smaller than the contribution from the Pomeron exchange amplitude of Eq. (49). At large momentum transfers with $|t| \sim |t|_{\text{max}}$ the resonant channel becomes essential.

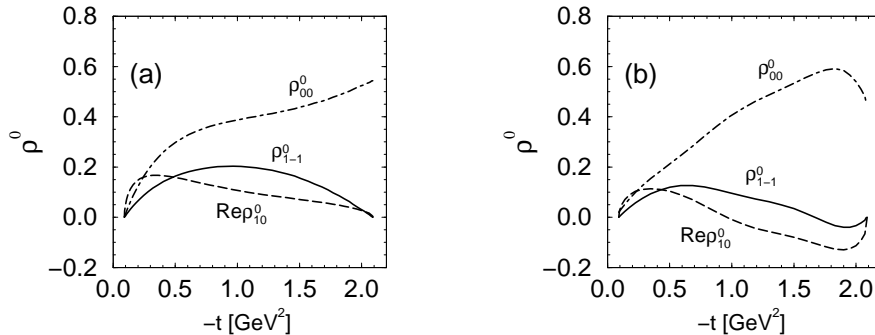


FIG. 6: Spin-density matrix elements ρ_{00}^0 , ρ_{10}^0 and ρ_{1-1}^0 for reaction $\gamma p \rightarrow \phi p$ as a function of $-t$ at $E_\gamma = 2.2 \text{ GeV}$ shown as dot-dashed, solid and dashed lines, respectively. (a): Result for the Pomeron exchange amplitude; (b): Result for the full model.

In Fig. 6 we show the t -dependence of the three ρ^0 matrix elements at $E_\gamma = 2.2 \text{ GeV}$. ρ^0 defines the angular distribution of K^+K^- -mesons in reactions with unpolarized photons (Eqs. (10), (14)). Fig. 6(a) is for the pure Pomeron exchange amplitude (Eq. (23)) and Fig. 6(b) for the full model which includes diffractive part, PS-meson-exchange and resonance excitations. One can see that for the full model the non-zero values of these spin-density matrix elements at forward angles photoproduction ($|t| < 1 \text{ GeV}^2$) are mostly determined by the Pomeron-exchange contribution. At large momentum transfers the resonant excitations play a key role.

The one-dimensional angular distributions $W^0(\cos \Theta)$ and $W^0(\Phi)$ at three values of $|t| = 0.2, 0.5$ and 1.8 GeV^2 are shown in Figs. 7(a) and (b), respectively. For small momentum transfers ($|t| \lesssim 0.2 \text{ GeV}^2$), the ϕ -mesons are produced transversely with its spin aligned along the quantization axis \mathbf{z}' ($\rho_{00}^0 \lll 1$). This results in the angular distribution $W^0(\cos \Theta) \simeq \sin^2 \Theta$. When $|t|$ increases, the spin-flip processes generate longitudinally-polarized ϕ -mesons (ρ_{00}^0 becomes finite). Initially, this leads to depolarization of the ϕ -mesons with $W^0(\cos \Theta) \simeq 0.5$ at $|t| \sim 0.5 - 0.6 \text{ GeV}^2$, and then, at large momentum transfers, to a predominance of the longitudinal polarization with $W^0(\cos \Theta) \simeq a + b \cos^2 \Theta$, where $a, b > 0$.

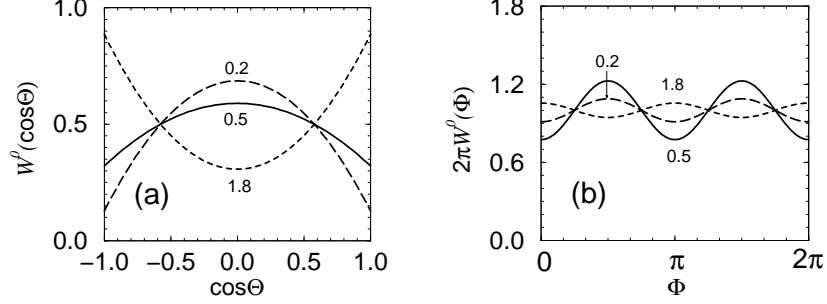


FIG. 7: The angular distribution of the ϕ -meson decay in reaction $\gamma p \rightarrow \phi p$ with unpolarized photon beam at $E_\gamma = 2.2$ GeV and $|t| = 0.2, 0.5$ and 1.8 GeV² (a): The dependence on $\cos\Theta$ (integrated over the azimuthal angle Φ); (b): The dependence on Φ (integrated over $\cos\Theta$).

The Φ -dependence of W^0 is determined completely by the double-spin-flip processes. The amplitude of the azimuthal-angle modulation is proportional to $2\rho_{1-1}^0$. It is exactly zero at $\theta = 0$ ($|t| = |t|_{\min}$), increases with increasing $|t|$ and reaches its maximum value at $|t| \simeq 0.6$ GeV². It goes down at large momentum transfers, as it is shown in Fig. 7(b). It is important to note, that the spin-conserving scalar and pseudoscalar-exchange processes do not contribute to ρ_{1-1}^0 . The contribution of the tensor part of f'_2 (square brackets in (38b)) and the resonant channel at $|t| \lesssim 0.8$ GeV² are rather small. Therefore, the distribution $W^0(\Phi)$ may be used as a tool to study dynamics of the spin-orbital interaction generated by the gluon-exchange processes in diffractive amplitude. At large momentum transfers $W^0(\cos\Theta)$, and $W^0(\Phi)$ are sensitive to the resonant channel.

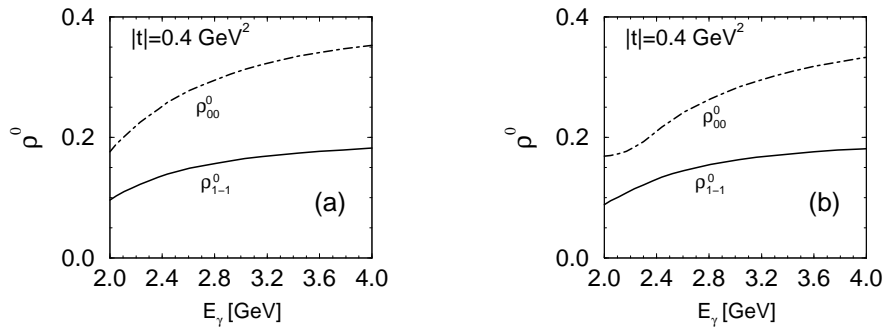


FIG. 8: Spin-density matrix elements ρ_{00}^0 and ρ_{1-1}^0 for reaction $\gamma p \rightarrow \phi p$ as a function of E_γ at $|t| = 0.4$ GeV². (a): Result for the Pomeron exchange amplitude; (b): Result for the full model.

Fig. 8 displays the energy dependence of the matrix elements ρ_{00}^0 and ρ_{1-1}^0 which define the one-dimensional distributions $W^0(\cos\Theta)$ and $W^0(\Phi)$, respectively, at fixed $|t|$: $|t| = 0.4$

GeV². The left (a) and right (b) panels correspond to calculation for the Pomeron-exchange and for the full amplitudes, respectively. One can see that the energy dependence of the matrix elements in both cases is very similar to each other. The increase of ρ_{00}^0 with energy reflects definite increase of amount of the longitudinally polarized ϕ -mesons with energy. The increase of ρ_{1-1}^0 with energy results in increasing the amplitude of the Φ -modulation in $W(\Phi)$.

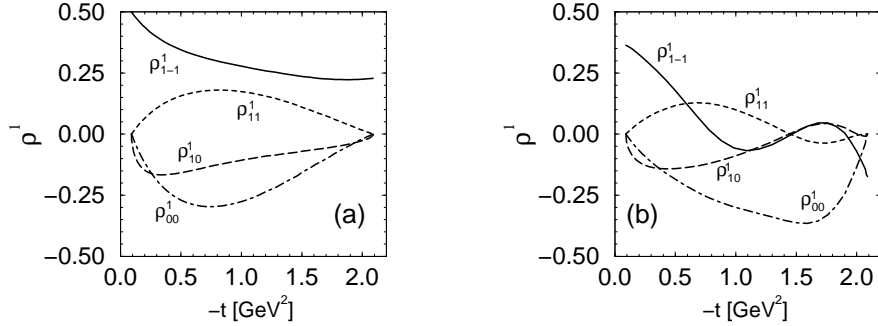


FIG. 9: Spin-density matrix elements ρ_{00}^1 , ρ_{11}^1 , ρ_{10}^1 and ρ_{1-1}^1 for reaction $\gamma p \rightarrow \phi p$ as a function of $-t$ at $E_\gamma = 2.2$ GeV. (a): Result for the Pomeron-exchange amplitude; (b): Result for the full model.

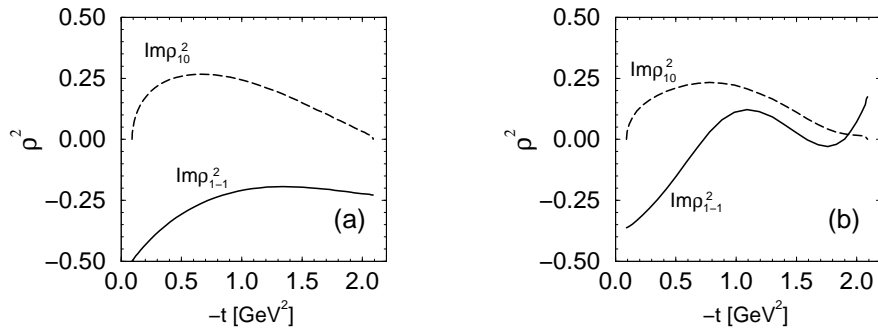


FIG. 10: Spin-density matrix elements $\text{Im}\rho_{10}^2$ and $\text{Im}\rho_{1-1}^2$ for reaction $\gamma p \rightarrow \phi p$ as a function of $-t$ at $E_\gamma = 2.2$ GeV. (a): Result for the Pomeron exchange amplitude; (b): Result for the full model.

Figs. 9 and 10 display the t -dependence of the matrix elements of ρ^1 and ρ^2 matrices, respectively. These matrix elements represent the angular distribution of K^+K^- -mesons in reactions with the linearly polarized photons (cf. Eqs. (12), (17)). Notation is the same as in Fig. 6. Consider first the matrix element ρ_{1-1}^1 . In the case of the helicity conserving model of Eq. (49), its meaning is the asymmetry in the contribution from natural and

unnatural-parity exchange parts

$$\rho_{1-1}^1 = \frac{1}{2} \frac{|I_0^N|^2 - |I_0^U|^2}{|I_0^N|^2 + |I_0^U|^2}. \quad (52)$$

Therefore, it is considered as a good tool to extract the relative contributions of the unnatural-parity-exchange processes from the angular distribution $W^L(\Phi - \Psi)$. However, the existence of spin-flip processes violates this identity and instead of Eq. (52) one has to use

$$\rho_{1-1}^1 = \frac{1}{2} \frac{|I_0^N|^2 - |I_0^U|^2 + |I_1^{1-1}|^2}{|I_0^N|^2 + |I_0^U|^2 + |I^{10}|^2 + |I_2^{1-1}|^2}, \quad (53)$$

where $|I^{10}|^2 = \text{Tr}[I_{\alpha;10} I_{\alpha;10}^\dagger]$ is the spin-contribution for transitions $\lambda_\gamma \rightarrow \lambda_\phi = 0$; $|I_1^{\alpha;1-1}|^2 = \text{Tr}[I_{\alpha;1-1} I_{\alpha;-11}^\dagger]$ and $|I_2^{\alpha;1-1}|^2 = \text{Tr}[I_{\alpha;1-1} I_{\alpha;1-1}^\dagger]$ are the spin-flip contributions for transitions $\lambda_\gamma \rightarrow \lambda_\phi = -\lambda_\gamma$. Only at $\theta = 0$ ($|t| = |t|_{\min}$) and $\rho_{00}^0 \simeq 0$ equations (52) and (53) are equivalent to each other.

For the pure Pomeron-exchange amplitude the contribution of the double-spin-flip can be estimated as

$$\frac{1}{N} |I_1^{1-1}|^2 \simeq \frac{1}{N} |I_2^{1-1}|^2 \simeq \frac{1}{2(1 - \rho_{00}^0)} (\rho_{1-1}^0)^2 \ll \rho_{00}^0, \quad (54)$$

where N is the normalization factor, defined by Eq. (7). Therefore, for the pure Pomeron-exchange amplitude we get the relation

$$\rho_{1-1}^1 \simeq \frac{1}{2} (1 - \rho_{00}^0) \quad (55)$$

which is confirmed by the explicit calculation of ρ_{00}^0 and ρ_{1-1}^1 , see in Figs. 6(a) and 9(a): ρ_{1-1}^1 decreases from $\frac{1}{2}$ at $|t| = |t|_{\min}$ to 0.23 at $|t| = |t|_{\max}$.

For the forward-angle photoproduction, where the contribution of the resonant channel to $|I^{1-1}|^2$ remains negligible, we get the following relation between ρ_{1-1}^1 and the relative contribution of the spin-conserving unnatural-parity-exchange amplitude

$$|\alpha^U|^2 \simeq \frac{|I_0^U|^2}{|I_0^N|^2 + |I_0^U|^2 + |I^{10}|^2}, \quad (56)$$

which can be rewritten as

$$|\alpha^U|^2 \simeq \frac{1}{2} (1 - 2\rho_{1-1}^1 - \rho_{00}^0). \quad (57)$$

This means that for evaluation of the relative contribution of the unnatural-parity exchange part from the data with a linearly polarized beam at small momentum transfers one has to account for ρ_{00}^0 , which in turn is extracted from the analysis of $W^0(\cos \Theta)$. At large $|t|$, ρ_{1-1}^1 is determined by the interplay between the resonant and all other channels and has no simple meaning.

Using the definition of spin-density matrices in Eqs. 6 one can get the following relation

$$-\text{Im}\rho_{1-1}^2 \simeq \rho_{1-1}^1 - \frac{(\rho_{1-1}^0)^2}{1 - \rho_{00}^0}. \quad (58)$$

Therefore, in Eq. (15), $\bar{\rho}_{1-1}^1 \simeq \rho_{1-1}^1$ and $\Delta_{1-1} \simeq 0$. So, the term proportional to $\cos[2(\Phi + \Psi)]$ in Eq. (15) is negligible.

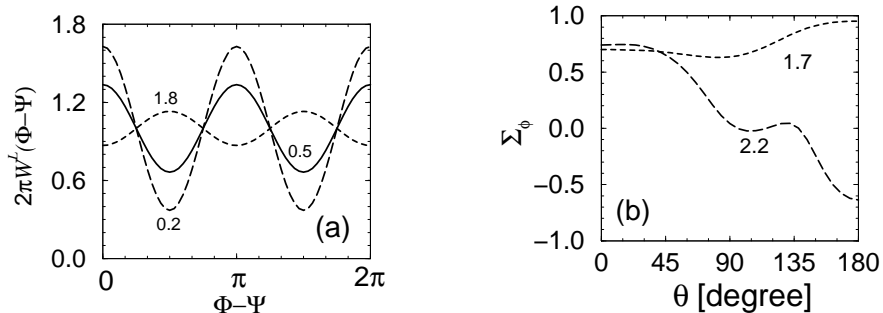


FIG. 11: (a): The angular distribution of the ϕ -meson decay as a function of $\Phi - \Psi$ in reaction $\gamma p \rightarrow \phi p$ with linear polarized photon beam at $E_\gamma = 2.2$ GeV and $-t = 0.2, 0.5$ and 1.8 GeV². b: The ϕ -meson decay asymmetry for $\gamma p \rightarrow \phi p$ reaction at $E_\gamma = 1.7$ and 2.2 GeV.

Fig. 11(a) shows the angular distribution $W^L(\Phi - \Psi)$ at $|t| = 0.2, 0.5$ and 1.8 GeV² ($E_\gamma = 2.2$ GeV). The amplitude of modulation of this distribution is equal to $2P_\gamma \rho_{1-1}^1$. In calculation we use $P_\gamma = 0.95$ which is reasonable for the highly-polarized photon beam at the LEPS of SPring-8 [62]. The amplitude of modulation has a maximum value at forward angles and decreases with increasing $|t|$.

Fig. 11(b) displays the ϕ -meson decay asymmetry Σ_ϕ (20), as a function of production angle θ . It is determined by the matrix elements $\rho_{1-1}^{1,0}$ and $\rho_{11}^{1,0}$. For the pure helicity-conserving amplitude there exist an identity: $\Sigma_\phi = 2\rho_{1-1}^1$. But in spin-flip processes this relation is violated. The scale of the violation increases with $|t|$. At large $|t|$, the shape of Σ_ϕ is sensitive to the resonant amplitude.

The decay distribution as a function of $\cos \Theta$ for the linearly polarized beam depends on the beam-polarization angle Ψ and matrix elements ρ_{11}^1 and ρ_{00}^1 (cf. Eq.15). In Fig. 12

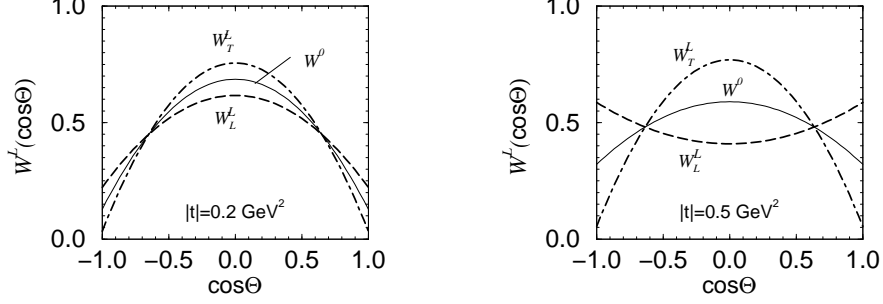


FIG. 12: The ϕ -meson decay distribution in reaction $\gamma p \rightarrow \phi p$ with linear polarized photon beam at $E_\gamma = 2.2$ GeV for vertical beam polarization with $\Psi = \frac{\pi}{2}$ (W_T^L) and horizontal polarization with $\Psi = 0$ (W_L^L) at $|t| = 0.2$ (a) and 0.5 GeV² (b).

we show result for the calculation of $W_L^L(\cos \Theta) \equiv W^L(\cos \Theta, \Psi = 0)$ and $W_T^L(\cos \Theta) \equiv W^L(\cos \Theta, \Psi = \frac{\pi}{2})$ at $|t| = 0.2$ GeV² and $|t| = 0.5$ GeV²: left (a) and right (b) panels, respectively. Also, for comparison, results for the angular distributions with an unpolarized beam are shown (thin solid lines). The difference between W_L^L and W_T^L disappears at $|t| \simeq |t|_{\min}$, but becomes very large at finite $|t|$. Using these distributions, one can extract ρ_{00}^1 and ρ_{11}^1 from the data:

$$\begin{aligned} \rho_{00}^1 &= \frac{1}{3P_\gamma} (W_T^L(\Theta = 0) - W_L^L(\Theta = 0)) \\ \rho_{11}^1 &= \frac{1}{3P_\gamma} (W_T^L(\Theta = \frac{\pi}{2}) - W_L^L(\Theta = \frac{\pi}{2})). \end{aligned} \quad (59)$$

The decay distribution as a function of the beam-polarization angle Ψ is defined by the matrix elements ρ_{11}^1 and ρ_{00}^1 . These matrix elements, taken separately, are finite at $|t| \neq |t|_{\min}, |t|_{\max}$. But the absolute value of the sum $2\rho_{11}^1 + \rho_{00}^1$ in Eqs. (18) is very small at forward-angle photoproduction

$$2\rho_{11}^1 + \rho_{00}^1 \simeq 0, \quad (60)$$

and becomes sizeable only at large momentum transfers. Eq. (60) allows to express the angular distribution for the linearly polarized beam $W^L(\cos \Theta, \Psi)$ similarly to the distribution for unpolarized beam $W^0(\cos \Theta)$

$$W^L(\cos \Theta, \Psi) = \frac{3}{2} \left(\frac{1}{2} (1 - \rho_{00}^{\text{eff}}) \sin^2 \Theta + \rho_{00}^{\text{eff}} \cos^2 \Theta \right), \quad (61)$$

where

$$\rho_{00}^{\text{eff}} = \rho_{00}^0 - P_\gamma \rho_{00}^1 \cos(2\Psi). \quad (62)$$

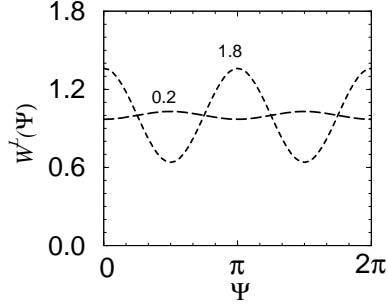


FIG. 13: The total ϕ -meson decay distribution in reaction $\gamma p \rightarrow \phi p$ with linear polarized photon beam at $E_\gamma = 2.2$ GeV and $-t = 0.2$ and 1.8 GeV² as a function of the angle between the beam polarization and production planes.

Fig. 13 shows the calculation of the total decay distribution as a function of the beam polarization angle Ψ . It is defined by sum $2\rho_{11}^1 + \rho_{00}^1$ (cf. Eq. 18), which is finite only at large momentum transfers. Here the sign and the amplitude of $W^L(\Psi)$ is determined by the resonant channels and prediction in this region is sensitive to the underlying theoretical model for the resonance part. The beam asymmetry Σ_x of Eq. (4) is related to $W^L(\Psi)$ as

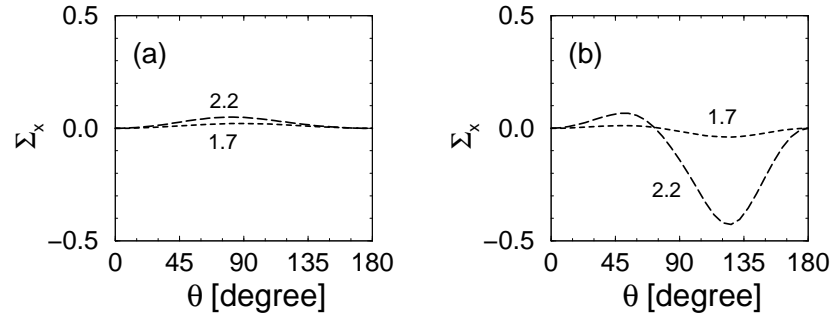


FIG. 14: The beam asymmetry for $\gamma p \rightarrow \phi p$ reaction at $E_\gamma = 1.7$ and 2.2 GeV. (a): Result for the Pomeron exchange channel; (b): Result for the full model.

$$\Sigma_x = \frac{W^L(\frac{\pi}{2}) - W^L(0)}{W^L(\frac{\pi}{2}) + W^L(0)} \quad (63)$$

and for the pure Pomeron exchange channel is defined by the interference of the first and third terms in (30) and can be evaluated in c.m.s. as

$$\Sigma_x \simeq \frac{q^2 \sin^2 \theta}{2\bar{s}}. \quad (64)$$

It is positive and increases near threshold with energy as q^2 (proportional to increase of the phase space), but remains small: $\Sigma_x \ll 1$. For the full model, the dominant contribution to Σ_x at large $|t|$ comes from the resonant channel. Thus, at $|t| \sim 1.8$ GeV ($E_\gamma = 2.2$ GeV), Σ_x becomes to be negative with large absolute value. This is illustrated in Fig. 14 where we show Σ_x , calculated for the pure Pomeron exchange amplitude and for the full model at the left (a) and the right (b) panels, respectively.

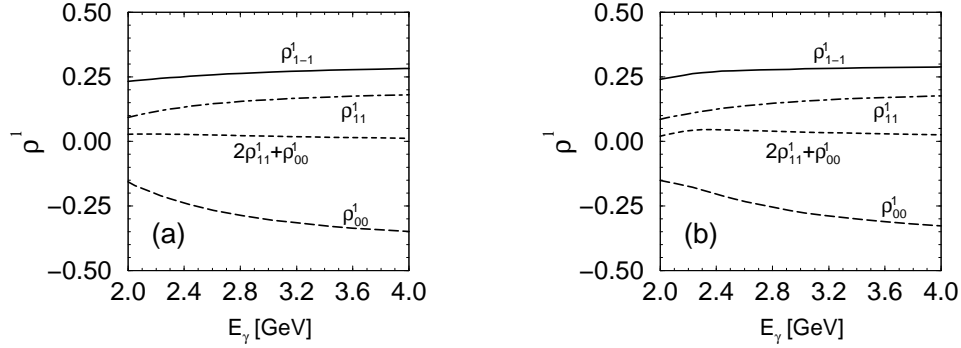


FIG. 15: Spin-density matrix elements ρ_{00}^1 , ρ_{11}^1 , ρ_{1-1}^1 , and sum of $2\rho_{11}^1 + \rho_{00}^1$ for reaction $\gamma p \rightarrow \phi p$ as a function of E_γ at $|t| = 0.4$ GeV². (a): Result for the Pomeron exchange amplitude; (b): Result for the full model.

Fig. 15 displays the energy dependence of the most important matrix elements, which define the angular distributions of $\phi \rightarrow K^+ K^-$ -decay with the linearly polarized photon beam and the beam asymmetry. The left (a) and right (b) panels correspond to the calculation for the Pomeron-exchange and for the full amplitudes, respectively. The energy dependence of ρ_{00}^1 and ρ_{11}^1 in both cases is similar to each other. The difference in ρ_{1-1}^1 is explained by the contribution of unnatural parity $\pi - \eta$ -meson exchange in the total amplitude. The calculation results in some decrease of ρ_{1-1}^1 and ρ_{00}^1 ; increase of ρ_{11}^1 , and almost constant value for $2\rho_{11}^1 + \rho_{00}^1 \simeq 0$.

Unfortunately, the available experimental data on the spin-density matrix elements $\rho^{1,2}$ in ϕ -meson photoproduction at $E_\gamma \sim 2 - 5$ GeV [57] are of a pure accuracy to make some definite conclusion about the photoproduction mechanism. To increase statistics they are combined at two energies (2.8 and 4.7 GeV) with momentum transfers $0.02 \leq |t| \leq 0.8$ GeV². The data are given in helicity frame where the spin-density matrix elements have additional kinematical dependence on the momentum transfers compared to the GJ-system [20]. In Table 1 we show the comparison of this data with our calculation for the "central" point

$E_\gamma = 3.75$ GeV and $|t| = 0.4$ GeV² in the helicity frame. One can see that the theoretical values are within experimental accuracy. Exception is ρ_{1-1}^1 , where the calculated value (0.44) exceeds the experimental one (0.18 ± 0.13) by two standard deviations. But close inspection shows some inconsistent with the data. Really, following the identity of Eq. (58) and using experimental values of $(\rho_{00}^0, \rho_{1-1}^0)$, one could expect $\rho_{1-1}^1 \sim -\text{Im}\rho_{1-1}^2$, i.e it must be close to 0.5 which is also supported by Fig. 29 of [57]. Nevertheless, it is clear, that for better understanding of details of the photoproduction processes the more precise experimental data in a wide kinematical region are desired.

The spin-density matrix elements ρ^3 , responsible for the angular distribution with the circularly polarized beam are shown in Fig. 16. They reach their maximum values

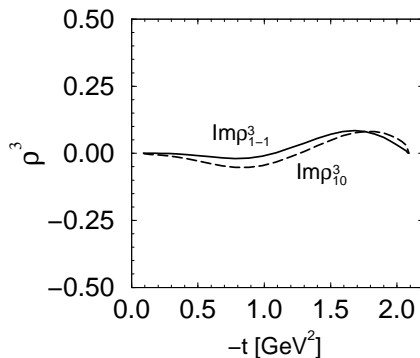


FIG. 16: Spin-density matrix elements $\text{Im}\rho_{10}^3$ and $\text{Im}\rho_{1-1}^3$ for the reaction $\gamma p \rightarrow \phi p$ as a function of $-t$ at $E_\gamma = 2.2$ GeV for the full model.

$\text{Im}\rho_{1-1(10)}^3 \simeq 0.1$ at $|t| \sim 1.8$ GeV². The finite value of $\text{Im}\rho_{1-1}^3$ generates an additional term in the angular distribution according to Eq. (19): $\Delta W^\pm(\Phi) = \pm(P_\gamma/\pi) \text{Im}\rho_{1-1}^3 \sin 2\Phi$. At forward photoproduction angles this term is rather weak and $W^\pm(\Phi) \simeq W^0(\Phi)$.

Next, we investigate the beam-target asymmetry which may be studied in reactions with a circularly-polarized beam and polarized target. Using the notation of Eq. (5), the expression for helicity-conserving amplitudes (49) and neglecting spin-flip processes, we can estimate C_{BT} at forward-angle photoproduction as

$$C_{BT}(t_{\max}) \simeq 2|\alpha^U| \cos(\delta_N - \delta_U), \quad (65)$$

where δ_N, δ_U are the phases of the natural and unnatural-parity-exchange amplitudes, respectively. From this expression it looks very attractive to use C_{BT} as a tool for studying

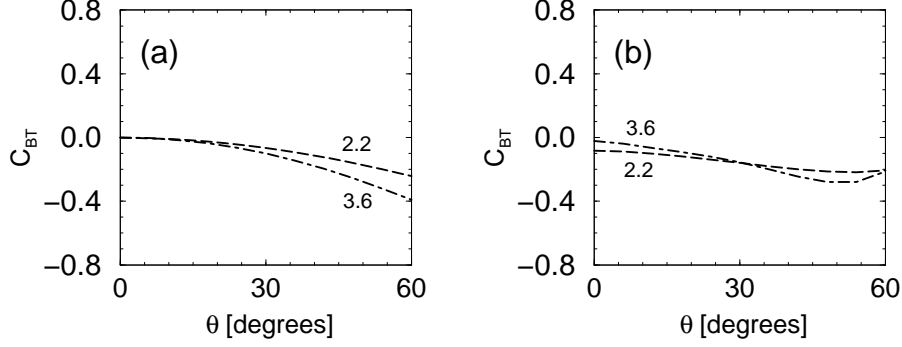


FIG. 17: The beam-target asymmetry for $E_\gamma = 2.2$ and 3.6 GeV at forward photoproduction angles. (a): Result for the Pomeron exchange amplitude; (b): Result for the full model.

contribution from exotic processes with unnatural-parity-exchange, because the asymmetry depends on α^U , but not on $|\alpha^U|^2$ [37].

However, analysis of the pure Pomeron-exchange amplitude shows that the second term of Eq. (30) gives some contribution to C_{BT} even without admixture of an unnatural-parity exchange component. This term contains a part which describes the interaction of the photon and proton spins which is governed by condition

$$\mathbf{s}_p + \boldsymbol{\lambda}_\gamma = \mathbf{s}_{p'}, \quad (66)$$

and select the initial state with the total spin $|\mathbf{s}_i| = \frac{1}{2}$. As a result, the beam-target asymmetry has an additional contribution

$$\Delta C_{BT} \simeq -\frac{(E_p + M_N)(E_{p'} + M_N)(n - n' \cos \theta)^2 (q(M_\phi^2 + |t|^2 + kM_\phi))^2}{4\bar{s}^2 (M_\phi(E_\phi + M_\phi))^2},$$

$$n = \sqrt{\frac{E_p - M_N}{E_p + M_N}}, \quad n' = \sqrt{\frac{E_{p'} - M_N}{E_{p'} + M_N}}. \quad (67)$$

Fortunately, at $E_\gamma = 2 - 3$ GeV and for $|t| \simeq |t|_{\min}$ this term is small and disappears with increasing E_γ . However, it is quite large at large momentum transfers. This is illustrated in Fig. 17 where we show calculations for the Pomeron-exchange amplitude and for the full model for $E_\gamma = 2.2$ and 3.6 GeV. At small $|t|$ and $E_\gamma \sim 2 - 3$ GeV the conventional processes considered above do not contribute to C_{BT} and it may be used as a tool to study the non-diffractive component with unnatural-parity exchange, like $s\bar{s}$ -knockout [37], etc. At large $|t|$ the beam-target asymmetry is defined by the interplay of all channels and is very sensitive to the production mechanism.

V. SUMMARY

In this paper we have discussed several topics of current interest for the ϕ meson photoproduction at low energies. In particular, we found that the spin-dependent interaction in the diffractive (Pomeron exchange) amplitude is responsible for the spin-flip transitions which are suppressed completely in the helicity-conserving processes. These transitions give sizeable contributions to the spin-density matrix elements and may be measured via the angular distributions of K^+K^- decays in reactions with unpolarized and polarized photons. Of special interest is the finite and large value of the ρ_{1-1}^0 matrix element generated by the double spin-flip transition. It is caused by the spin-orbital interaction inherent to the two-gluon exchange processes in the diffractive channel. This matrix element generates the Φ -dependence of the decay-angular distribution in reactions with unpolarized photons at forward angles. That is, the spin observables at small $|t|$ may be used as a tool for studying diffractive mechanism in detail.

Combined study of ϕ and ω photoproduction at large angles allows the analysis of the status of OZI-rule for ϕNN^* -interactions relative to the standard estimation based on the violation of $\phi - \omega$ mixing from its ideal value. We found a large (factor of 4) scale of this violation which agrees with other independent indications for this effect.

We also have shown that spin observables at large momentum transfers are due to the interplay between the resonant and all other channels, and therefore, may be used to test the resonance excitation mechanism, which is a issue of current interest.

It would be interesting to extend our analysis of spin-density matrix elements to the ω -photoproduction too. This needs to include into consideration additional channels like initial and final state interactions [55], direct quark exchange [54], contribution of the conventional meson trajectories [21] and others. This will be subject of future study.

Another interesting problem we have not investigated in this work is to use the spin observables to extract information about the exotic isoscalar processes, like $s\bar{s}$ -knockout [34, 37], G -poles [24], etc. with unnatural-parity-exchange properties. The most challenging question is to exclude the contribution of the pseudoscalar π -meson exchange. This problem may be solved in a combined study of the spin-density matrix elements measured using linearly-polarized photons and the beam-target and/or beam-recoil double polarizations measured using circularly-polarized photons on the proton and deuteron targets [63].

It is then possible to determine the absolute value and the phase of the "exotic channel". The corresponding theoretical estimations will be presented in our forthcoming paper.

Acknowledgments

We thank S. Date, H. Ejiri, M. Fujiwara, K. Hicks, T. Hotta, K. Mawatari, T. Mibe, T. Nakano, D.J. Tedeschi and R.G.T. Zegers for fruitful discussion. This work was supported in part by U.S. Department of Energy, Nuclear Division, Contract N^o W-31-109-ENG-38.

APPENDIX A: COMPARISON STUDIES OF DIFFRACTIVE MECHANISMS

Up to now we have discussed diffractive photoproduction, where the dominance contribution comes from the Pomeron exchange and the additional trajectories are added to improve the total unpolarized cross section at low energy. Let us denote this diffractive model as a model "P". As we discussed in Sect. III the finite value of threshold parameter $a_P \sim s_P$ in (40) eliminates the Pomeron contribution at $E_\gamma \sim 2$ GeV, which must be compensated by an increase of strength of the additional trajectories. The validity of different assumptions must be checked in study of the polarization observables in diffractive region, because the vertex functions for the Pomeron and other trajectories in Eqs. (27) - (38b) lead to different predictions. By way of illustration we shall compare the model "P", with the model "2⁺" which represents the f'_2 Regge trajectory and PS-meson exchange and the model "0⁺", which is the PS-meson exchange and the scalar (glueball-exchange) trajectory. The two last cases are realized if one choose the threshold parameter in (40) $a_P \simeq s_R \sim (M_N + M_\phi)^2$ and $a_{R \neq P} = 0$.

In Fig. 18 we show the differential cross section of $\gamma p \rightarrow \phi p$ reaction as a function of $-t$ at $E_\gamma = 2.2$ GeV for the three models together with the available experimental data [59]. Parameters of the Pomeron exchange amplitude are fixed from the high energy region, for other trajectories we use $g_{2^+} = 0.82 g_P$, and $g_{0^+} = 3.9 g_P$. The contribution of the pseudoscalar π, η -exchange is also shown for completeness. We also show case when the diffractive channel is built from the Pomeron and PS-exchanges. In this case the calculation is slightly below data. But all other three models are close to each other and it is difficult to distinguish between them using only unpolarized differential cross section. Situation reverses

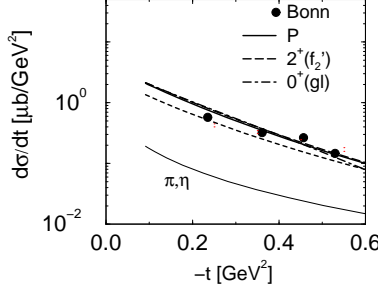


FIG. 18: (a): The differential cross section of $\gamma p \rightarrow \phi p$ reaction at $E_\gamma = 2.2$ GeV for the models "P", "2⁺" and "0⁺" indicated by solid dashed, and dot-dashed curves, respectively. The contribution of the pseudoscalar π, η -exchange is shown by the solid thin curve. The short dashed curve corresponds to the case when diffractive channel represents Pomeron and PS-exchange. Data are taken from Ref. [59]

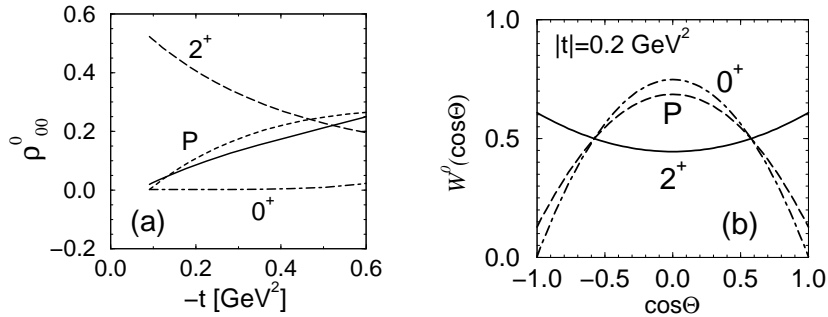


FIG. 19: The spin-density matrix element ρ_{00}^0 (a) and the angular distribution $W^0(\cos \Theta)$ (b) for the three models of diffractive ϕ -meson photoproduction. Notation is the same as in Fig. 18.

if we look at spin observables.

Fig. 19(a) shows ρ_{00}^0 for different models as a function of $-t$ at $E_\gamma = 2.2$ GeV. Thus, for the 0^+ -exchange $\rho_{00}^0 \simeq 0$, for the Pomeron exchange it increases monotonically with $|t|$. For 2^+ -exchange ρ_{00}^0 decreases with t , starting from a large value at $|t| = |t|_{\min}$, because of the spin-flip terms. They are the first and the third terms in the square brackets of (38b). These terms generate a finite value of ρ_{00}^0 even at forward angle photoproduction. The difference in ρ_{00}^0 leads to the difference in decay distribution $W^0(\cos \Theta)$ shown in Fig. 19(b) for $|t| = 0.2$ GeV². For 0^+ -exchange, ϕ -mesons produced to be transversely polarized, the Pomeron exchange process results in partial ϕ -meson "depolarization". In case of 2^+ -exchange we get rather strong ϕ -meson depolarization with an enhancement of the longitudinal polarization

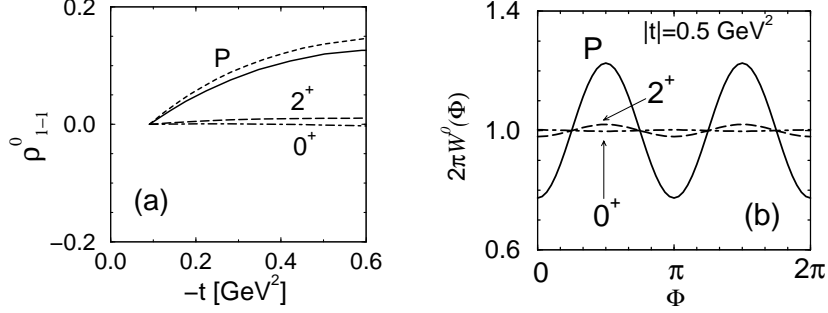


FIG. 20: The spin-density matrix element ρ_{1-1}^0 (a) and the angular distribution $W^0(\Phi)$ (b) for the three models of diffractive ϕ -meson photoproduction. Notation is the same as in Fig. 18.

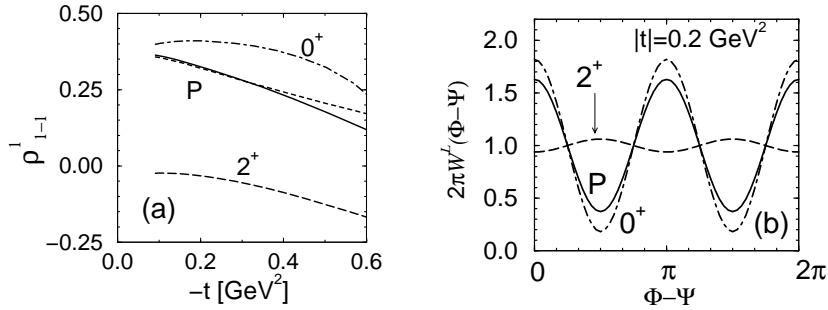


FIG. 21: The spin-density matrix element ρ_{1-1}^1 (a) and the angular distribution $W^L(\Phi-\Psi)$ (b) for the three models of diffractive ϕ -meson photoproduction with linearly polarized photons. Notation is the same as in Fig. 18.

at $|t| = |t|_{\min}$. One can also see, that the difference between "hybrid" model "P" (solid curve) in Fig. 19(a) and pure Pomeron-exchange model (short dashed curve) is negligible.

In Fig. 20(a) we show ρ_{1-1}^0 generated by the the double spin-flip transition $\lambda_\gamma \rightarrow \lambda_\phi = -\lambda_\gamma$. This matrix element is proportional to interference of helicity conserving and double spin-flip transition amplitudes and almost equal to zero for 0^+ -model. For "P" and 2^+ models it increases with $|t|$ monotonically, but in 2^+ -exchange it is much smaller.

As we have discussed above the matrix element ρ_{1-1}^1 depends on the contribution of unnatural parity exchange components and strength of the single-spin-flip component or ρ_{00}^0 (cf. Eq.(57)). In 2^+ -model the spin-conserving component or ρ_{11}^0 is dominated by PS-exchange and therefore the relative contribution of unnatural parity exchange is smaller then in other cases. Also ρ_{00}^0 is greater. This leads to strong decreasing of ρ_{1-1}^1 at forward angles up to the negative values, which is illustrated in Fig. 21(a). At small and finite $|t|$ this matrix element is the biggest for 0^+ - model, since there are no spin-flip processes in this

case. The corresponding angular distributions $W^L(\Phi - \Psi)$ at $|t| = 0.2 \text{ GeV}^2$ are shown in Fig. 21(b). One can see strong difference between 2^+ -exchange and other models. Existing data [57] support for the small value for ρ_{00}^0 and finite value for ρ_{1-1}^1 . This eliminates large component of 2^+ -exchange. In order to distinguish between Pomeron and 0^+ -exchange one needs at least data on ρ_{1-1}^0 -matrix element (cf. Fig. 20) which is crucial for these models on the qualitative level.

-
- [1] A. Donnachie and P.V. Landshoff, Phys. Lett. B **185**, 403 (1987); Nucl. Phys. **B244**, 322 (1984); *ibid.* **B267**, 690 (1986);
 - [2] P.V. Landshoff and O. Nachtmann, Z. Phys. C **35**, 405 (1987).
 - [3] S.V. Goloskokov, Phys. Lett. B **315**, 459 (1993).
 - [4] J.-M. Laget and R. Mendez-Galain, Nucl. Phys. **A581**, 397 (1995).
 - [5] M.A. Pichowsky and T.-S.H. Lee, Phys. Lett. B **379**, 1 (1996); Phys. Rev. D **56**, 1644 (1997).
 - [6] A. Hebecker and P.V. Landshoff, Phys. Lett. B **419**, 393 (1998).
 - [7] J.R. Cudell, K. Kang, and S. K. Kim, Phys. Lett. B **395**, 311 (1997).
 - [8] L.D. Solovev, Theor. Math. Phys. **126**, 203 (2001) [Teor. Mat.Fiz. **126**, 247 (2001)].
 - [9] Q. Zhao, Z. Li, and C. Bennhold, Phys. Lett. B **436**, 42 (1998); Phys. Rev. C **58**, 2393 (1998).
 - [10] Q. Zhao, J. P. Didelez, M. Guidal and E. Hourany, Nucl. Phys. A **684** (2001) 351.
 - [11] Q. Zhao, Phys. Rev. C **63** (2001) 025203.
 - [12] M. Post, U. Mosel, Nucl. Phys. A **688**, 808 (2001).
 - [13] Yongseok Oh, A. Titov and T.-S.H. Lee, Phys. Rev. C **63**, 025201 (2001).
 - [14] Q. Zhao, B. Saghai and J. S. Al-Khalili, Phys. Lett. B **509**, 231 (2001); Q. Zhao, arXiv:nucl-th/0202023.
 - [15] M. F. M. Lutz, Gy. Wolf and B. Friman nucl-th/0112052.
 - [16] A.I. Titov and T.-S.H. Lee, Phys. Rev. C, **66**, 015204 (2002).
 - [17] N. Isgur and G. Karl, Phys. Lett. B **72**, 109 (1977); Phys. Rev. D **18**, 4187 (1978); **19**, 2653 (1979); R. Koniuk and N. Isgur, *ibid.* **21**, 1868 (1980).
 - [18] S. Capstick, Phys. Rev. D **46**, 2864 (1992).
 - [19] S. Capstick and W. Roberts, Phys. Rev. D **49**, 4570 (1994).
 - [20] A. I. Titov, T.-S.H. Lee, H. Toki, and O. Streltsova, Phys. Rev. C **60**, 035205 (1999).

- [21] J.-M. Laget, Phys. Lett. B **489**, 3133 (2000);
- [22] R. A. Williams, Phys. Rev. C **57**, 223 (1998).
- [23] T. Nakano and H. Toki, in *Proceedings of the International Workshop on Existing Physics and New Accelerator Facilities*, SPring-8, Hyogo, 1997 (World Scientific Singapore, 1998), p.48.
- [24] N. I. Kochelev and V. Vento, Phys. Lett. B **515**, 375 (2001); hep-hp/0112292.
- [25] J. Ellis, M. Karliner, D.E. Kharzeev, and M.G. Sapozhnikov, Nucl. Phys. **A673**, 256, 2000; J. Ellis, Nucl. Phys. **A684**, 53, 2001.
- [26] H. Genz and G. Hölner, Phys. Lett. B **61**, 389 (1976).
- [27] R.L. Jaffer, Phys. Lett. B **229**, 275 (1989).
- [28] S.B. Gerasimov, Phys. Lett. B **357**, 666 (1995); Chin. J. Phys. (Taipei) **34**, 848 (1996).
- [29] S. Okubo, Phys. Lett. **5**, 165 (1963); G. Zweig, CERN Report No. 8182/TH 401 and 8419/TH 412, 1964 (unpublished); J. Iizuka, Prog. Theor. Phys. Supp. **37/38**, 21 (1966); G. Alexander, H.J. Lipkin, and P. Scheck, Phys. Rev. Lett. **17**, 412 (1966).
- [30] J. Gasser, H. Leutwyler, and M. E. Sainio, Phys. Lett. B **253**, 252 (1991).
- [31] ASTERIX Collaboration, J. Reifenrother *et al.*, Phys. Lett. B **267**, 299 (1991).
- [32] Crystal Barrel Collaboration, V.G. Ableev *et al.*, Nucl. Phys. A **585**, 577 (1995).
- [33] OBELIX Collaboration, A. Bertin *et al.*, Phys. Lett. B **388**, 450 (1996).
- [34] E.M. Henley, G. Krein, and A.G. Williams, Phys. Lett. B **281**, 178 (1992); E.M. Henley, T. Frederico, S.J. Pollock, S. Ying, G. Krein, and A.G. Williams, Few-Body Syst. (Suppl) **6**, 66 (1992).
- [35] M. Pichowsky, Ç. Şavkli, and F. Tabakin, Phys. Rev. C **53**, 593 (1996).
- [36] A. I. Titov, Y. Oh, and S. N. Yang, Phys. Rev. Lett. **79**, 1634 (1997).
- [37] A.I. Titov, Y. Oh, S.N. Yang, and T. Morii, Phys. Rev. C **58**, 2429 (1998); Nucl. Phys. **A684**, 354 (2001).
- [38] K. Hagiwara *et al.* [Particle Data Group Collaboration], Phys. Rev. D **66**, 010001 (2002).
- [39] K. Schilling, K. Seyboth and G. Wolf, Nucl. Phys. **B15**, 397 (1970).
- [40] P.D.V. Collins, *An introduction to Regge theory & high energy physics*, Cambridge University Press, London, New York, Melbourne, 1977.
- [41] P.D.V. Collins and E.J. Squires, *Regge poles in particle physics*, Springer Tracts in Modern Physics, V.45, Springer-Verlag Berlin Heidelberg New York, 1968.
- [42] A. Donnachie and R.G. Kirsopp, Nucl. Phys. **B10**, 433, (1969).

- [43] M. Diehl, Eur.Phys. J. C6, 503 (1999).
- [44] F.E. Low, Phys. Rev. D **12**, 163 (1975); S. Nussinov, Phys. Rev. Lett. **34**, 1286 (1975).
- [45] J.R. Cudell, A. Donnachie and P.V. Landshoff, Nucl. Phys. **B322**, 55 (1989).
- [46] M. G. Ryskin, Z. Phys. C **57**, 89 (1993).
- [47] J.R. Cudell and I. Royen, Phys. Lett. B **397**, 317 (1997).
- [48] B. Friman and M. Soyeur, Nucl. Phys. **A600**, 477 (1996).
- [49] M. Guidal, J.M. Laget, and M. Vanderhaegen, Nucl. Phys. **A627**, 645 (1997).
- [50] S.V. Talalov, arXiv:hep-ph/010128.
- [51] T. Sato and T.-S.H. Lee, Phys. Rev. C **54**, 2660 (1996).
- [52] M. Benmerrouche, N. C. Mukhopadhyay and J. F. Zhang, Phys. Rev. D **51**, 3237 (1995).
- [53] F. J. Klein, Ph.D. thesis, Bonn Univ. (1996); SAPHIR Collaboration, F. J. Klein *et al.*, π N Newslett. **14**, 141 (1998).
- [54] The CLAS Collaboration, M. Battaglieri, *et al.*, Phys. Rev. Lett. **90**, 022002 (2003).
- [55] Y. Oh and T.-S.H. Lee, Phys. Rev. C **66**, 045201 (2002).
- [56] A. Sibirtsev and W. Cassing, Eur. Phys. J. A **7**, 407, 2000.
- [57] J. Ballam *et al.*, Phys. Rev. D **7**, 3150 (1973).
- [58] D.P. Barber *et al.*, Z. Phys. C **12**, 1 (1982).
- [59] H.J. Besch, G. Hartmann, R. Kose, F.Krautschneider, W. Paul, and U. Trinks, Nucl. Phys. B **70**, 257 (1974).
- [60] The CLAS Collaboration, E. Anciant *et al.*, Phys. Rev. Lett. **85**, 4682 (2000).
- [61] D.J. Tedeschi *for the CLAS Collab.*, in Proc. of International Symposium *Electromagnetic Interactions in Nuclear and Hadron Physics. Osaka 2001* (World Scietific, 2002), p. 367.
- [62] T. Nakano *for the LEPS Collab.*, in Proc. of International Symposium *Electromagnetic Interactions in Nuclear and Hadron Physics. Osaka 2001* (World Scietific, 2002), p. 24.
- [63] A.I. Titov, M. Fujiwara, and T.-S.H. Lee Phys. Rev. C **66**, 022202 (2002).

TABLE I: Comparison of calculated spin density matrix elements in helicity system with experimental data of [57] at $E_\gamma = 2.8$ and 4.7 GeV for $0.02 \leq |t| \leq 0.8$ GeV². Theoretical prediction is done at $E_\gamma = 3.75$ and for $|t| = 0.4$ GeV².

$\rho_{\lambda\lambda'}$	Exper.	Calc.
ρ_{00}^0	-0.04 ± 0.06	0.061
$\text{Re}\rho_{10}^0$	-0.00 ± 0.06	-0.067
ρ_{1-1}^0	-0.04 ± 0.10	0.042
ρ_{00}^1	-0.13 ± 0.09	0.010
ρ_{11}^1	-0.06 ± 0.11	0.018
$\text{Re}\rho_{10}^1$	0.00 ± 0.09	0.063
ρ_{1-1}^1	0.18 ± 0.13	0.44
$\text{Im}\rho_{10}^2$	-0.02 ± 0.10	-0.052
$\text{Im}\rho_{1-1}^2$	-0.51 ± 0.16	-0.44